ABSTRACT

Title of dissertation: VACUUM PROPERTIES OF QCD
                           IN AN ELECTROMAGNETIC FIELD

                           Elizabeth Werbos, Doctor of Philosophy, 2009

Dissertation directed by: Professor Thomas D. Cohen
                              Department of Physics

The non-trivial vacuum properties of Quantum Chromodynamics can be affected by a constant external magnetic field. The chiral condensate and the magnetization of the vacuum are the two properties studied in this work. The chiral condensate, which is the order parameter for chiral symmetry breaking–one of the most important properties of QCD–is an optimal quantity to study at intermediate field strengths. Using both models and chiral perturbation theory, it can be shown that an electric field suppresses the chiral condensate whereas a magnetic field enhances it. Higher-order calculations in χPT may have a substantial effect on the magnitude of the shift in the chiral condensate, but their exact effect is unknown due to the uncertainty in the parameters of the theory. The second parameter, the magnetization, is used at fields large enough for perturbative calculations to be valid; at these scales, there is large explicit chiral symmetry breaking and the chiral condensate cannot be used. The first-order magnetization shows a correction of the form $B \log B$; the calculation to next order in perturbation theory shows a correction small enough that non-perturbative corrections dominate.

VACUUM PROPERTIES OF QCD IN AN ELECTROMAGNETIC FIELD

by

Elizabeth Werbos

Dissertation submitted to the Faculty of the Graduate School of the
University of Maryland, College Park in partial fulfillment
of the requirements for the degree of
Doctor of Philosophy
2009

Advisory Committee:
Professor Thomas D. Cohen, Chair/Advisor
Professor Paulo Bedaque
Professor Elizabeth J. Beise
Professor Alice C. Mignerey
Professor Stephen J. Wallace

Acknowledgments

My experience in graduate school has been smoother than I expected when I first entered, in large part due to the kind support of those around me.

I would first and foremost like to thank my advisor, Tom Cohen. He is a tireless advocate and friend for his students, as well as being an excellent scientist, and I count myself lucky to have worked with him.

In addition, I would like to thank the other members of the TQHN group, whose enthusiasm for science fosters an atmosphere encouraging cooperation and intellectual inquiry. In particular, I would like to thank my additional direct collaborators, Aleksey Cherman and David McGady.

I would also like to gratefully acknowledge the support of the administrative staff in the Physics department. In particular, I would like to thank Loretta Robinette, who, among many other things, has kindly provided editorial corrections for my papers, and Jane Hessing, who made the administrative aspect of the program run smoothly.

My family, as well, has provided a great deal of support in all aspects of my life, and I am grateful to them for providing me with the resources to have carried me this far in life.

I would also like to thank my many friends for providing the community and stability necessary in any life endeavor.

Finally, I thank DOE for their support via grant number DE-FG02-93ER-40762.

Table of Contents

List of Figures

Chapter 1

Introduction

The study of physics has progressed over time from the study of the very large to the study of progressively smaller scales. Our understanding of the composition of matter has deepened from molecules, to nuclei, to the protons and neutrons composing them, and finally to the fundamental degrees of freedom for the interactions of these hadrons, quarks, governed by Quantum Chromodynamics (QCD). The discussion which follows and the rest of the introduction follow closely, in many cases, the discussions in textbooks such as refs. [2, 3]. More details can be found in these and other sources.

In QCD, the vacuum, or absence of real particles, is nontrivial, and so it is valuable to analyze the effects of external conditions on this vacuum. This work discusses the effects of an external electromagnetic field on this vacuum in a variety of energy regimes.

The following chapter contains a discussion of QCD as a theory. It begins with the origins of QCD, its structure and pertinent features, and the experimental results which have confirmed this structure. This is followed by a discussion of the methods of calculating in QCD at various energy regimes. Finally, a brief overview of the features of the QCD vacuum and how it is affected by external parameters is given. Chapt. 2 discusses the effects of an external electromagnetic field of low-to-

medium strength using models and the leading order in Chiral Perturbation Theory. Chapt. 3 extends the Chiral Perturbation Theory result to next-to-leading order. Chapt. 4 discusses the effects of a strong electromagnetic field on the QCD vacuum.

1.1   The Brief Story of QCD

The transition from an understanding in terms of hadrons to one in terms of quarks is interesting because it was driven by mathematical necessity as well as by direct experimental observation. The observed hadrons fit very well into representations of the flavor symmetry group $SU(3)_F$, but none transformed as the fundamental representation of this group[4, 5]. Mathematically, all representations can be ultimately decomposed in terms of the fundamental representations of their group, and so it is natural to postulate a corresponding physical object, the quark, which must be a fermion. Nature is only approximately symmetric with respect to flavor, and we know now that the three light quark flavors in this approximate symmetry group (up, down, strange) are supplemented by additional flavors with much larger masses (charm, bottom, top).

The quark model [4] was developed from these needs and proved very successful at explaining the menagerie of known hadrons, but left a few puzzles. Notably, no candidate particles with fractional charge had been discovered, and one baryon, the Δ^{++}, would be a completely symmetric bound state of quarks[6, 7, 8, 9]–an impossibility for fermions. In order to resolve these difficulties, *color*, an extra degree of freedom, was introduced[10, 11, 8]. Each quark, in addition to its other

quantum numbers, has one of three colors. The underlying theory is completely symmetric with respect to this degree of freedom. Therefore, the wave function for a baryon, can be completely antisymmetric with respect to color, making it possible for the rest of the wave function to be completely symmetric.

Color also provides a natural framework for the notion of *confinement*, the fact that although quarks fit well with mathematical necessity, no free quarks were observed. It is postulated that observable particles must be in a completely antisymmetric, "white," color state. Not only does color allow a more precise description of a confined state, but it also leads to at least a qualitative understanding for why confined states are required. This is closely related to another important feature of QCD–*asymptotic freedom*[12, 13], the weakening of the QCD coupling at high energies. Asymptotic freedom is a natural consequence of a scale anomaly at the quantum level of the theory.

Real understanding of the strong force requires a precise formulation of the lagrangian for the theory. Construction of the QCD lagrangian was guided by a few principles: it must respect the known symmetries of nature, and exhibit all experimentally observed features. Conveniently, the idea of color fits seamlessly into an already existing sophisticated mathematical framework, that of *non-abelian gauge theories* or Yang-Mills theories[14].

Mathematically, the color symmetry corresponds to the invariance of the lagrangian under transformations in the color symmetry group, $SU(3)_C$. Quarks naturally transform under the fundamental representation of this group, undergoing the transformation $\psi(x) \rightarrow e^{i\alpha^a t^a}\psi(x)$, where α^a is an arbitrary parameter multiply-

ing the (non-Abelian, non-commuting) generators of the group, t^a, and $\psi(x)$ is the quark field. The *global* form, where α^a is taken to be constant over space, is simple to implement. However, from the study of quantum electrodynamics (QED), it was clear that *local* symmetries, where $\alpha^a = \alpha^a(x)$, are potentially interesting, and lead to a rich dynamical theory[15]. The derivative in the kinetic term acts on this transformation when it is applied locally, and in order to keep the lagrangian invariant, a new position-dependent operator must be introduced–for the non-Abelian group $SU(3)$ this is the gluon field. As the gauge field for QCD, the gluon moderates the strong interactions just as the photon and the $W^{\pm}$ and Z^0 bosons moderate the electromagnetic interaction. The QCD lagrangian can be written[3, 16]

$$\mathcal{L}_{QCD} = -\frac{1}{4}G_a^{\mu\nu}G_{\mu\nu}^a + i\bar{\psi}_j^\alpha \gamma^\mu \left(D_\mu\right)_{\alpha\beta} \psi_j^\beta - m_j\bar{\psi}_j^\alpha \psi_{j,\alpha}, \qquad (1.1)$$

where $G_{\mu\nu}^a \equiv \delta_\mu A_\nu^a - \delta_\nu A_\mu^a + gf_{abc}A_\mu^b A_\nu^c$, $\psi(x)$ and $\bar{\psi}(x)$ are the quark and anti-quark fields, and $(D_\mu)_{\alpha\beta} \equiv \delta_{\alpha\beta}\partial_\mu - ig\sum_a \frac{1}{2}\lambda_{\alpha\beta}^a A_\mu^a$, with α and β representing color indices. The matrices $\lambda_{\alpha\beta}^a$ are the eight 3×3 generators of the color group, and the f_{abc} are the structure constants of the $SU(3)$ algebra, $[T_a, T_b] = if_{abc}T_c$, with $(T^a)_{\alpha\beta} = \frac{1}{2}\lambda_{\alpha\beta}^a$.

One difference between QED and QCD which can be read from the lagrangian is that in QCD, the gauge bosons can interact with each other in three-gluon and four-gluon vertices.

More importantly, the peculiar nature of the non-Abelian QCD interaction leads to a key feature of QCD, asymptotic freedom [12, 13]. It is well known that couplings in quantum field theory vary by the scale at which interactions take place. In QED, this can be qualitatively understood as "screening." Virtual electron-

positron pairs cluster around each source of charge. When an interaction takes place at a long distance (low momentum), the source of charge appears screened (reduced) by these extra pairs. However, closer to the charge carrier, its "bare" charge is manifest, and in fact becomes infinite as the interaction becomes arbitrarily close. By contrast, in non-Abelian gauge theories, the opposite occurs, and the charge is anti-screened, with the interaction appearing weaker at short distances. The qualitative picture for this is more complex, but its difference with QED is, as expected, a result of the presence of three different colors interacting in a non-Abelian way.

Asymptotic freedom is the result of this anti-screening effect in which at small distances (high energy), QCD becomes weak, in contrast with QED, which becomes strong at small distances and weak at long distances. Philosophically, asymptotic freedom is desirable. A theory which is asymptotically free is formally valid up to any energy and can thus be treated as a fundamental theory in its own right, regardless of its range of validity in nature. In contrast, a theory like QED is thought to make sense only as an effective theory, since the theory is presumably not well defined at short distances and high energies due to the diverging coupling in that regime. By contrast, anti-screening makes the QCD coupling increase with distance, which provides an intuitive picture of confinement. Qualitatively, as two colored charges move away from each other, the potential between them becomes so great that a new pair of colored charges is created from the vacuum, cancelling the members of the original pair and forcing the whole system to appear colorless.

The QCD lagrangian fits all of the requisite properties of a theory of the strong

interactions, but the final test is to see if it produces verifiable numbers in agreement with experiment. Asymptotic freedom allows perturbative calculations in QCD at very high energy, which is where persuasive tests of the theory occur. Scattering of a lepton off of a nucleon (Deep Inelastic Scattering, DIS) is a measurable process where the scaling of the QCD coupling at various energy scales becomes apparent. Such experiments give strong experimental evidence that QCD is indeed correct at high energies. The theory behind this scaling will be discussed briefly below.

The corollary, that the QCD coupling becomes large at low energies, makes calculation more difficult at these low energies. Not only is experimental verification at these energies not possible, it is difficult to gain understanding of any kind at these energies. Numerous methods and models have sprung up which will be discussed later.

1.2   Calculating in QCD

With the QCD lagrangian, the theory of the strong force can be said to be formally "known," but it is of no practical use without the ability to make predictions that can be tested against experiment. Because the QCD coupling is different in various energy regimes, the method for making these concrete predictions will vary. This section discusses the most important of these methods, divided by energy regime.

At high energies QCD is perturbative, and calculations are simple to perform; this is the regime which produces the precise results which have been used

to verify QCD. At the very lowest energies, it is possible to constrain the number of possible terms in the "effective" lagrangian to a manageable number, constraining their relative strength through experiment using Chiral Perturbation Theory (χPT)[17, 18, 19]. In between, a number of less rigorous methods have been conceived, including the NJL model and related models[20], the linear sigma model[21], the large-N_C expansion[22, 23, 24], and recent attempts to apply the AdS/CFT correspondence to QCD[25].

1.2.1 High-energy: Perturbative QCD

QCD is perturbative, and so calculations at high energy follow the same procedure as any field theory calculation. Following is a brief discussion of some of the more important results.

The calculation of the running of the QCD coupling which leads to asymptotic freedom demonstrates one of the most important features of QCD. As with any quantum field theory, the Callan-Symanzik equation[26, 27] is used to calculate the β-function as a function of the coupling. In QCD, the β-function can be calculated at lowest non-trival order to be

$$\beta(g) = -\frac{g^3}{(4\pi)^2}b_0,$$

(1.2)

where the strong coupling $\alpha_s = g^2/4\pi$ and $b_0 \equiv \left(\frac{11}{3}N_C - \frac{2}{3}N_f\right)$; N_C is the number of colors (three in the real world) and N_f is the number of flavors (generally three, but more at energies above the masses of the heavier quark flavors). This leads to

an equation for the running coupling of the form

$$\alpha_s(Q) = \frac{\alpha_s(\mu)}{1 + (b_0 \alpha_s(\mu)/2\pi) \log(Q/\mu)}. \tag{1.3}$$

This is all the information required to calculate the coupling of QCD at any scale, but lacks any fixed parameters. The dimensionless coupling can run and thus is not an essential characteristic of the theory. In addition, the arbitrarily defined renormalization scale, μ, has entered the problem. The solution is to define the QCD scale, Λ_{QCD}, via

$$1 = \alpha_s b_0/(2\pi) \log(\mu/\Lambda_{QCD}). \tag{1.4}$$

The relationship between a running dimensionless parameter and an arbitrary renormalization scale has been neatly encapsulated into a single physically meaningful scale, which can help us gain insight into the workings of QCD. It is this scale which determines whether calculations can be performed perturbatively or whether lower-energy methodology must be used. Λ_{QCD} is a parameter of the theory and must be determined from experiment.

It is also worth noting that any observable quantity must be independent of unphysical scales, so it must also obey a Callan-Symanzik equation, with the running dependent on the coupling constant evaluated at whatever relevant scales; if there is only one, that is the scale which determines whether the perturbative expansion is valid or not.

Another important effect of the running of the QCD constant is scaling violation. Bjorken scaling[28] (no change in coupling with scale) is derived in the limit where there are no interactions between quarks. High energy collisions close to this

limit are in the regime where QCD is perturbative, and so QCD corrections can be calculated. The Altarelli-Parisi equations[29], which describe the evolution of the nucleon structure functions over x, cannot be analytically solved but can be evolved numerically over x. The results of this evolution are in persuasive agreement with experiment, as can be seen in Fig. 1.2.1[30].

Numerous perturbative QCD processes can and have been calculated. Some of the most important can be found in textbooks such as Refs. [2, 3].

1.2.2   Low-energy: Chiral Perturbation Theory

On the opposite end of the spectrum from high energy QCD, α_s becomes strong and we might expect that calculations would be absolutely impossible except by brute force methods such as lattice QCD[31]. This is largely true at medium energies, but at low energies the situation is simplified. Here, the energy is so low that the higher-energy degrees of freedom are "frozen," and the only relevant degrees of freedom are the pions whose dynamics are explained using Chiral Perturbation Theory (χPT)[17, 18, 19]. There are a number of good reviews covering the basics of χPT in some depth, including, for example, Refs. [32, 33]. Much of this section follows closely the discussion in Ref. [33].

To understand χPT, it is important to first understand chiral symmetry. It acts on the isospin doublet

$$\psi = \begin{pmatrix} u \\ d \end{pmatrix}.$$

(1.5)

The plot shows $F_2(x,Q^2) * 2^{i_x}$ on the vertical axis versus $Q^2 \ (GeV^2)$ on the horizontal axis.

Proton

★ H1
● ZEUS
✚ BCDMS
○ E665
□ NMC
△ SLAC

x=0.000063
x=0.000102
x=0.000162
x=0.000253
x=0.0004
x=0.0005
x=0.000632
x=0.0008
x=0.00102
x=0.0013
x=0.00161
x=0.0021
x=0.00253
x=0.0032
x=0.005
x=0.008
x=0.013
x=0.021
x=0.032
x=0.05
x=0.08
x=0.13
x=0.18
x=0.25
x=0.4
x=0.65
x=0.75
x=0.85 (i_x=1)
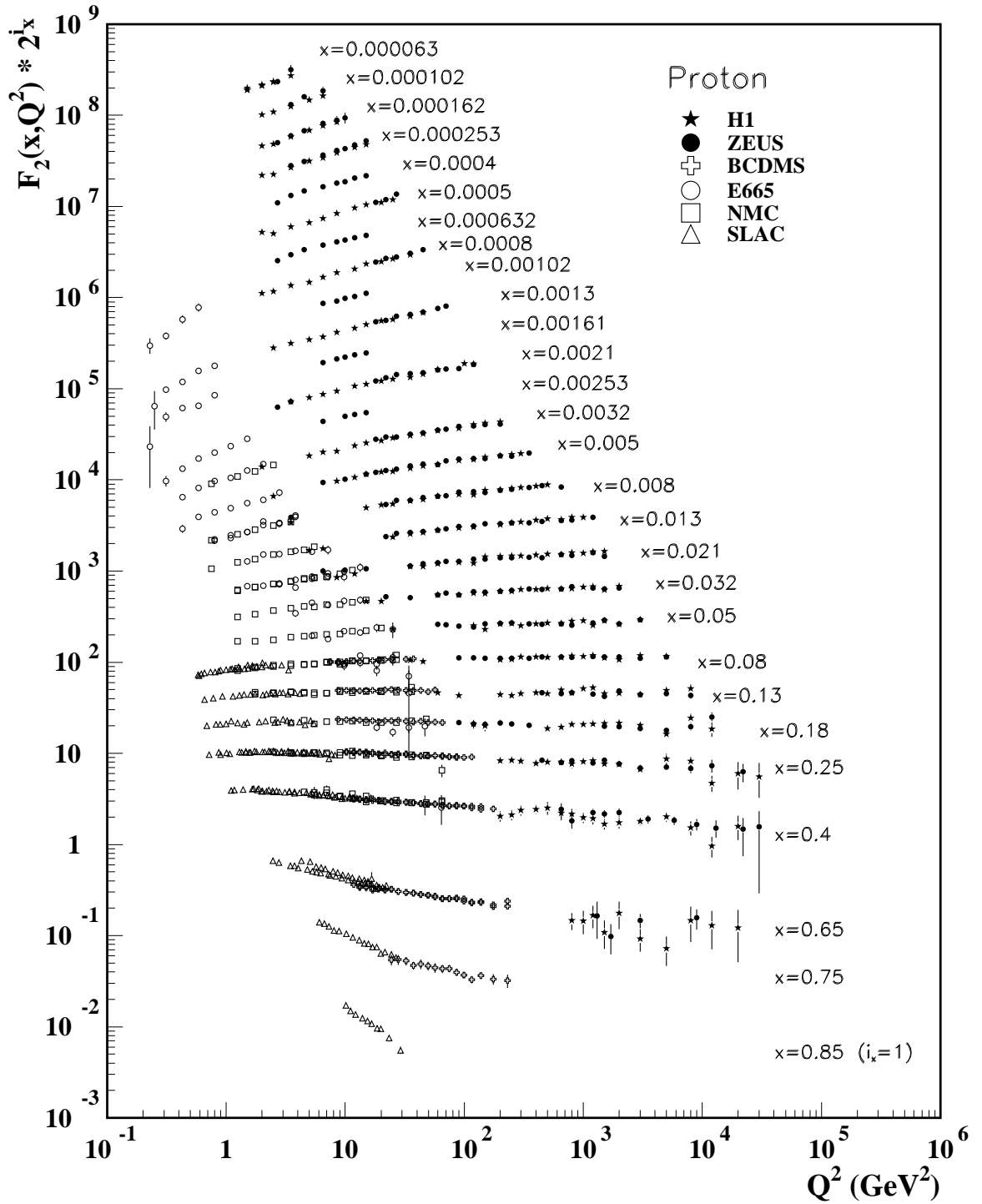
Figure 1.1: The evolution of the structure function F_2 with x and Q^2

10

Quark fields can be expressed more conveniently in terms of their "chirality" as

$$\psi_L(x) = \frac{1}{2}(1 - \gamma^5)\psi(x) \qquad \psi_R(x) = \frac{1}{2}(1 + \gamma^5)\psi(x), \tag{1.6}$$

where ψ_L is termed the "left-handed" field and ψ_R is the "right-handed" field. Rewriting the QCD lagrangian for massless quarks in terms of these fields results in independent terms for ψ_L and ψ_R; the two different kinds of chiral transformations correspond to these fields undergoing separate chiral transformations. Thus, the lagrangian has more symmetry than could naively be expected. This symmetry, $SU(2)_L \times SU(2)_R$ (or $SU(3)_L \times SU(3)_R$ if the slightly heavier strange quark is incorporated), can be written in terms of the quark fields as the two independent transformations

$$\psi(x) \rightarrow e^{i\alpha}\psi(x) \qquad \psi(x) \rightarrow e^{i\alpha\gamma^5}\psi(x). \tag{1.7}$$

Chiral symmetry is not exact; the quark mass term is mixed in left- and right-handed quark fields, so that the small quark mass results in a slight breaking of chiral symmetry. However, more interesting than this slight breaking is the large *spontaneous* breaking of chiral symmetry which takes place in the QCD vacuum. The *chiral condensate,*

$$\Sigma = \langle \bar{q}q \rangle = \langle 0 | \bar{q}q | 0 \rangle = \langle 0 | \bar{q}_L q_R + \bar{q}_R q_L | 0 \rangle \tag{1.8}$$

is not invariant under separate left- and right-handed chiral rotations. Thus, if the QCD vacuum is really almost invariant under separate chiral rotations, we would expect this quantity to be very near zero. The measurement and interpretation of the chiral condensate requires some care, as it is a scale-dependent quantity. Still,

11

with this in mind, it can be measured as $-(229 \pm 9\mathrm{M}eV)^3$ at 1 GeV[34]. This value is much larger than we would expect from the slight breaking of chiral symmetry due to the quark mass, and therefore chiral symmetry must be spontaneously broken. Goldstone's theorem says that for every spontaneously broken continuous symmetry, there will be a massless particle with the quantum numbers of the symmetry rotation[35], so it is critical to find out exactly how many symmetries are broken in this case. While the chiral condensate is not invariant with respect to independent rotations of the left- and right-handed quarks, it is invariant with respect to the same rotation of both. The symmetry breaking then takes the form $SU(2)_L \times SU(2)_R \to SU(2)_{L+R}$. Four independent symmetries are broken, and we should look for massless particles which correspond to these symmetries. There are no exactly massless particles with the appropriate quantum numbers, but there are particles with unexpectedly low masses, the pseudoscalar triplet of pions. Their small mass can be attributed to the small quark masses; in the absence of quark masses and with exact chiral symmetry they would be massless.

It is now clear why pions are the ideal degrees of freedom for chiral perturbation theory. Pions are mesons, which can be identified as the Goldstone bosons of spontaneous chiral symmetry breaking, which gives them a mass markedly lower than other scales in QCD. This scale separation allows the expansion parameter m_π/Λ to be small (where Λ is the next largest scale). This expansion is Chiral Perturbation Theory (χPT)[17, 18, 19], one of a general class of theories called effective theories (see [36] for a review).

At energies close to the pion mass, it will be convenient to model QCD in-

teractions as interactions between pions. As with all effective theories, the kinds of interactions (terms in the Lagrangian) that are possible will be limited by the symmetries of the problem. The expansion parameter, p/Λ, provides a framework for ordering these possible interactions. The terms at lowest order in the momentum (m_π, p, or external terms such as the electromagnetic field) will give dominant contributions to the calculation. These constraints together restrict the lowest orders of the chiral lagrangian to a manageable number of terms. Each of these terms represents an interaction allowed by the symmetries of the problem. The relative strength of these interactions, however, is undetermined by χPT; it must somehow be dictated by the details of higher-energy physics. The only dependence on this high-energy physics is encapsulated into the "low-energy coefficients" (LECs) which multiply each term in the lagrangian.

The chiral lagrangian can most easily be constructed by using building blocks which naturally carry the symmetries of the problem. For the $SU(2)$ case, the pion octet can be combined into a unitary matrix U using the Weinberg parameterization,

$$U = \sigma + \frac{i}{F_\pi}\vec{\tau}\cdot\vec{\pi} \qquad \sigma^2 + \frac{\vec{\pi}^2}{F_\pi^2} = 1. \tag{1.9}$$

Here, the pions are still the independent degrees of freedom, and σ can be expanded in terms of the pion fields based on the second equation. The U matrix transforms linearly under a chiral transformation, but because of the nonlinear relationship between U and π due to the second relation, the pions do not. The U matrix is the most elementary building block for the lagrangian, but since $U^\dagger U = 1$, a nontrivial lagrangian will require at least a derivative, which contributes a factor of p, the

momentum. The lowest-order lagrangian possible is

$$\mathcal{L}_2 = \frac{f^2}{4}\langle\partial_\mu U^\dagger\partial^\mu U\rangle, \tag{1.10}$$

where $\langle A\rangle$ indicates a trace, and f is a dimensionful parameter that is yet to be determined. For concrete calculations, U must be expanded in terms of the pion fields; each term in that expansion will be smaller by a factor of $\vec{\pi}/F_\pi$. For calculations involving only $\mathcal{L}_2$, only the first term in this expansion can be used. Higher order terms in the U expansion will also require higher order terms in the lagrangian.

χPT also needs a way to incorporate the relevant parameters of QCD, such as m_π, and external fields, such as the electromagnetic fields. This is neatly accomplished by incorporating these parameters as classical background sources. This corresponds to modifying the original QCD lagrangian to be

$$\mathcal{L}_{QCD} = \mathcal{L}_{QCD}^0 + \bar{q}\gamma^\mu(v_\mu + \gamma^5 a_\mu)q - \bar{q}(s - i\gamma^5 p)q, \tag{1.11}$$

where these external fields are taken to be probes. Using the standard background field method, Green's functions and expectation values for other quantities can be calculated by varying the generating functional with these external fields and taking the zero-field limit of this variation. The generating functional is written in terms of the quark and gluon fields

$$\exp\{iZ\} = \int \mathcal{D}q\mathcal{D}\bar{q}\mathcal{D}\mathcal{G}_\mu \exp\left\{i\int d^4x\mathcal{L}_{QCD}\right\}. \tag{1.12}$$

This functional becomes S_2, the classical action at lowest order.

The concept of gauge invariance can be used to extend the background fields to the χPT formulation. The QCD lagrangian with these backgrounds obeys global

14

symmetry transformations, which when promoted to local symmetries require the

chiral lagrangian to contain the fields a_μ and v_μ within the constructions

$$D_\mu U = \partial_\mu U - ir_\mu U + iU l_\mu$$

$$D_\mu U^\dagger = \partial_\mu U^\dagger + iU^\dagger r_\mu - il_\mu U^\dagger$$

$$F_L^{\mu\nu} = \partial^\mu l^\nu - \partial^\nu l^\mu - i[l^\mu, l^\nu] \tag{1.13}$$

$$F_R^{\mu\nu} = \partial^\mu r^\nu - \partial^\nu r^\mu - i[r^\mu, r^\nu].$$

In the isospin limit (the regime used here) $l_\mu = r_\mu$ and thus $F_L = F_R$. The param-

eters s and p are not separately gauge invariant, but the combination $s + ip$ is, so

these external fields must appear together in that form. The independent values of

s and ip are arbitrary, so without loss of generality, the $p = 0$ gauge can be chosen.

In the isospin limit ($m_u = m_d$) of $SU(2)$ these background fields can be iden-

tified in terms of the parameters we are interested in as

$$r_u \equiv v_\mu + a_\mu = eQA_\mu + \ldots$$

$$l_u \equiv v_\mu - a_\mu = eQA_\mu + \ldots \tag{1.14}$$

$$s = \mathcal{M} + \ldots,$$

where Q and $\mathcal{M}$ are the charge and mass matrices for the quarks.

Finally, the most general lowest-order lagrangian using all of these components

is

$$\mathcal{L}_2 = \frac{f^2}{4} \langle D_\mu U^\dagger D^\mu U + U^\dagger \chi + \chi^\dagger U \rangle, \tag{1.15}$$

where $\chi = 2B_0(s + ip)$, with B_0 a constant which will be determined later. With

nonzero external fields, chiral symmetry is broken, but because the symmetries of

the original theory have been preserved, this breaking takes the same form as that in the QCD lagrangian.

Armed with the lowest order lagrangian, it is possible to relate the constants appearing in χPT to the parameters of QCD. The two constants at this level are f and B_0. The first step is expanding the $\mathcal{L}_2$ lagrangian in terms of the pion fields. In particular, the mass terms are (again, taking the isospin limit $m_u = m_d = m_q$)

$$\mathcal{L}_{mass}^{(2)} = -m_q B_0 (\pi^0)^2 - 2m_q B_0 \pi^+ \pi^-. \tag{1.16}$$

The pion mass can then immediately be identified as

$$m_\pi^2 = 2m_q B_0. \tag{1.17}$$

Other identifications can be obtained from the generating functional (1.12). The pion coupling constant, f_π, can be obtained from its definition and this generating functional as

$$i\sqrt{2} f_\pi p^\mu \equiv \langle 0 | (J_A^\mu)^{12} | \pi^+ \rangle = \frac{\delta S_2}{\delta a_\mu}, \tag{1.18}$$

which results in the identification $f = f_\pi$.

Following these calculations, in the Weinberg parameterization and the isospin limit, the lowest order lagrangian can be written in terms of the pion fields as

$$L^{(2)} = \frac{1}{2} (\partial_\mu \pi^0)^2 - \frac{M_\pi^2}{2} (\pi^0)^2 + (\partial_\mu \pi^+ + ieA_\mu \pi^+)(\partial_\mu \pi^- - ieA_\mu \pi^-) - M_\pi^2 \pi^+ \pi^-$$
$$+ \frac{1}{2F_\pi^2} \left[\pi^0 \partial_\mu \pi^0 + \partial_\mu (\pi^+ \pi^-) \right]^2 - \frac{M_\pi^2}{8F_\pi^2} \left[2\pi^+ \pi^- + (\pi^0)^2 \right]^2.$$

$$\tag{1.19}$$

The situation with the $\mathcal{L}^{(4)}$ is somewhat more complex. First, it can be constructed using the same principles as $\mathcal{L}^{(2)}$, but has more terms and therefore more undetermined LECs. Another difference is that while the LECs at the lowest order, F and

16

M, have an obvious interpretation in terms of physical quantities, the coefficients at higher orders must be extracted indirectly from experimental processes or the lattice. In these results, the $SU(3)$ LECs are most often quoted. The full form of the next order lagrangian using the $SU(3)$ U matrix is

$$
\begin{aligned}
\mathcal{L}^{(4)} =& L_1 \langle D_\mu U^\dagger D^\mu U \rangle^2 + L_2 \langle D_\mu U^\dagger D_\nu U \rangle \langle D^\mu U^\dagger D^\nu U \rangle \\
& + L_3 \langle D_\mu U^\dagger D^\mu U D_\nu U^\dagger D^\nu U \rangle + L_4 \langle D_\mu U^\dagger D^\mu U \rangle \langle U^\dagger \chi + \chi^\dagger U \rangle \\
& + L_5 \langle D_\mu U^\dagger D^\mu U \left(U^\dagger \chi + \chi^\dagger U \right) \rangle + L_6 \langle U^\dagger \chi + \chi^\dagger U \rangle^2 \\
& + L_7 \langle U^\dagger \chi - \chi^\dagger U \rangle^2 + L_8 \langle \chi^\dagger U \chi^\dagger U + U^\dagger \chi U^\dagger \chi \rangle \\
& - i L_9 \langle F_R^{\mu\nu} D_\mu U D_\nu U^\dagger + F_L^{\mu\nu} D_\mu U^\dagger D_\nu U \rangle + L_{10} \langle U^\dagger F_R^{\mu\nu} U F_{L\mu\nu} \rangle \\
& + H_1 \langle F_{R\mu\nu} F_R^{\mu\nu} + F_{L\mu\nu} F_L^{\mu\nu} \rangle + H_2 \langle \chi^\dagger \chi \rangle.
\end{aligned}
\tag{1.20}
$$

The form of $\mathcal{L}^{(4)}$ is greatly simplified using only two quark flavors ($SU(2)$) and in the isospin limit. The relationship between the $SU(2)$ and $SU(3)$ LECs is:

$$
\begin{aligned}
l_1 =& 4L_1 + 2L_3 \qquad l_2 = 4L_2 \qquad l_3 = 4(-2L_4 - L_5 + 4L_6 + 2L_8) \\
l_4 =& 4(2L_4 + L_5) \qquad l_5 = L_1 0 \qquad l_6 = -2L_9 \\
l_7 =& -8(2L_7 + L_8).
\end{aligned}
\tag{1.21}
$$

The LECs H_1 and H_2 multiply terms with no pseudoscalar fields, and so are not directly measurable.

The chiral expansion has been extended to $O(p^6)$[37, 38], with 115, 94, or 57 terms, for $SU(n)$, $SU(3)$, and $SU(2)$, respectively. It will not be reproduced in full here, but select terms will be used in calculation later.

In general, χPT predictions have good agreement with experimental and numerical lattice data, with some observables accurately reproduced at $O(p^4)$, and

others requiring $O(p^6)$ calculations to be accurately modeled (see Ref. [39] for a review of some results).

One of the most useful applications of χPT is in lattice QCD. Due to the limitations of computational power, lattice calculations are often made with unrealistic values for physical QCD parameters, such as M_π. Rather than outputting results with as little meaning as the unphysical masses that are input, lattice calculations can instead be used to obtain values for the LECs, which are independent of the unphysical QCD inputs[40, 41]. These LECs can then be used with more realistic QCD values to obtain concrete predictions for the real world.

1.2.3 Medium energy: Models and the Lattice

At energies approaching Λ_H, neither pQCD nor χPT can give reliable predictions. Numerous models are used to try to close this gap, including the NJL model, the linear-σ model, applications of AdS/CFT, and others, with the large-N_C approximation helping to guide the selection of models. While model-building has up until now been the only analytical strategy for understanding QCD, numerical calculation in the form of lattice QCD[31] has come to the forefront in theoretical understanding (for a recent review of basic lattice results see Ref. [42]).

1.2.3.1 The large N_C approximation

The QCD coupling constant is not small at medium energies, and therefore an expansion in α_s is not perturbative. Naively, one might hope to make a perturbative

expansion in some alternative parameter. In the 1970s, 't Hooft and Witten[22, 23, 24] identified an unlikely alternative for a small expansion parameter: $1/N_C$, where N_C is the number of colors and is taken to increase from $3 \to \infty$. In this case, the color symmetry group is $SU(N_C)$, and the gluon field has N_C^2 components, and the quark field has N_C components. On its face, this approximation is not very good; $N_C = 3$ in the real world. Nonetheless, the hope is that the large-N_C approximation can provide some level of qualitative understanding in a regime where there is a dearth of analytical tools.

The next step is to understand where N_C appears in QCD. There is some explicit N_C dependence: A closed quark loop, for example, can be of any color and therefore results in an extra factor of N_C. Other parameters–the QCD coupling constant g, in particular–may or may not have N_C dependence, and so the large-N_C expansion is, on some level, inherently arbitrary. This choice can be made somewhat intelligently by deciding which quantities should have a smooth limit for $N_C \to \infty$. In the canonical 't Hooft large N_C limit, the gluon one-loop vacuum polarization (Fig. 1.2(a)) is taken to have a smooth large-N_C limit. In this diagram, the gluon contributes an explicit factor of N_C^2, but because of the constraints of the external lines, the diagram has an overall explicit factor of N_C. The two vertices contribute a factor of g^2, so any total N_C dependence would come from the combination $g^2 N_C$, called the 't Hooft coupling. For a smooth N_C limit, this factor must be N_C independent, which requires the dependence $g \propto 1/\sqrt{N_C}$.
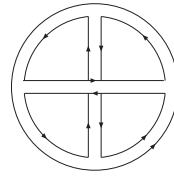
Once the N_C dependence of the coupling has been determined, it is possible to make some deductions about the behavior of fields in this limit. A convenient
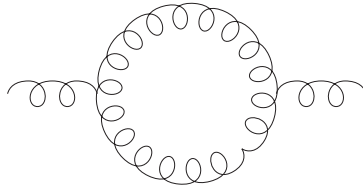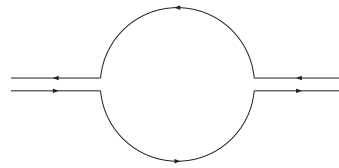
(a) lowest-order gluon vacuum
polarization
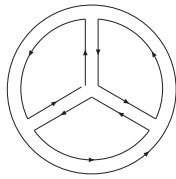
(b) a planar diagram

(c) a non-planar diagram
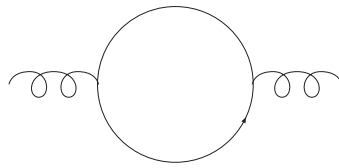
(d) Quark one-loop correction to gluon vacuum polarization
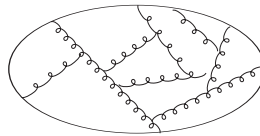
(e) Meson at large-N_C

Figure 1.2: Large N_C diagrams

tool for making these deductions is the "double line notation" of 't Hooft[22], where particles can be represented by a number of lines corresponding to their color degrees of freedom; thus, quarks and anti-quarks are represented by a single line and gluons are represented by a double line. In this notation, then, a closed loop will contribute a factor of N_C, and a vertex will contribute a factor of $1/\sqrt{N_C}$ from the coupling constant. Before moving on to the properties of mesons, it is possible to list a few rules determining which diagrams will contribute to a process.

The first of these is the rule that non-planar diagrams are suppressed. Examples of planar and non-planar diagrams in double-line notation can be seen in Figs. 1.2(b) and 1.2(c). The planar diagram carries a factor of $N_C^3(1/\sqrt{N_C})^4 = N_C$, whereas the non-planar diagram carries a factor of $N_C^1(1/\sqrt{N_C})^4 = 1/N_C$. This property can be understood in general by considering the iterative insertion of gluons. If a gluon is inserted into a planar diagram to produce another planar diagram, it is either dividing one loop into two loops (on the inside) or adding a loop where there was none (on the outside). Thus, the net change in the N_C dependence of the diagram is $N_C(1/\sqrt{N_C})^2 = 1$. On the other hand, if the insertion of a gluon produces a non-planar diagram, it will have combined two loops into a single loop, with a total change of at least $1/N_C(1/\sqrt{N_C})^2 = 1/N_C^2$.

The other selection rule is that internal quark lines are suppressed. This can be roughly understood by noting that a closed quark loop has N_C degrees of freedom, and a closed gluon loop has N_C^2 degrees of freedom, which will lead to diagrams containing these loops to be down by one order of N_C. The particular case of a single quark loop in the gluon propagator can be seen in Fig. 1.2(d), with

21

N_C dependence $(1/\sqrt{N_C})^2 = 1/N_C$. However, rather than understanding this rule in the context of a quark loop as a gluon loop minus one N_C term, it is fruitful to examine the comparison of a diagram with no internal quark loop to one which has one. Here, inserting a quark loop within a single gluon propagator will result in two new orders of the coupling constant, but will not change the number of loops in the diagram (attaching other gluons to the loop will have the same effect as discussed above and will not change the N_C dependence). Thus, internal quark lines are suppressed.

Unfortunately, while the number of diagrams can be reduced in the large-N_C limit, there is still an infinite number, so exact calculation of the contributing diagrams at large-N_C is not practical. Even with just the N_C dependence, however, it is still possible to make some interesting deductions from the large-N_C limit.

Using these rules, a clear picture of the composition of a meson at large-N_C emerges. It will look something like Fig. 1.2(e), with a single external quark line and an arbitrary number of gluons in a planar arrangement within it. Similarly, any process composed of initial and final mesons must have the same structure with the same overall N_C dependence. From this, it is straightforward to find the N_C dependence of meson sources and of meson interactions. In fact, as discussed in more detail in Ref. [24], intermediate states in diagrams of this form (as represented by a "cut" across a diagram), must be color singlets with the quantum number of mesons.

More concretely, $J(x)$ can be defined as a current with the quantum numbers to create a meson. The fact that any intermediate state must be a one-meson state

means that

$$\int d^4x e^{-ikx} \langle T J(x) J(0) \rangle = \sum_n \frac{a_n^2}{k^2 - m_n^2},$$ (1.22)

where $a_n = \langle 0|J|n \rangle$. The only N_C dependence here is from a_n, and since the overall N_C dependence of the diagram is $O(N_C)$, $a_n \propto \sqrt{N_C}$. The N_C dependence of meson interactions can then be deduced. The three-point function $\langle JJJ \rangle$ is represented by a similar diagram with three meson creation currents. Because the intermediate states must similarly be single-meson states, the amplitude will be of the form $\langle 0|J|m \rangle^3 \Gamma_{mmm}$. It can quickly be deduced, then, that $\Gamma_{mmm} \propto 1/\sqrt{N_C}$. An n-meson interaction vertex will have a similar form, $\langle 0|J|m \rangle^n \Gamma_{(n)}$, with $\Gamma_{(n)} \propto N_C^{1-\frac{n}{2}}$.

Thus, interactions between any number of mesons disappear at large-N_C and therefore mesons are non-interacting. Following similar logic, it can be shown that both mesons and gluons are stable, free, and non-interacting as $N_C \rightarrow \infty$, and that they do not mix. The analysis for baryons is more complicated[24], but the result is that baryons have masses which diverge with N_C and finite interaction cross-sections.

Another curious consequence of these properties is that at large-N_C the number of mesons becomes infinite. In perturbative QCD, the two-point function of eqn. (1.22) is proportional to $\log k^2$, and since every individual resonance is distinct and is only proportional to $1/k^2$, the only way to get the necessary momentum dependence is with an infinite number of states.

With these basic properties, it is possible to make an assessment of how well the behavior in the large-N_C approximation describes the behavior of mesons in

the real world. Some of the original reasons why the large-N_C approximation was attractive are outlined by Ref. [24]. One of the most obvious is Zweig's rule, which states that diagrams for meson processes that can be cut by crossing only internal gluon lines are suppressed. This rule becomes exact at large-N_C, where mixing between gluons and mesons disappears. Zweig's rule is observed in phenomenology, but the only theoretical explanation comes from the large-N_C limit. Another important feature reproducing reality follows closely on the basic rule that internal quark loops are suppressed. This indicates that the $\bar{q}q$ sea is suppressed, which is true in phenomenology. The non-interaction of mesons has two other verifiable results; first, that exotics, which can be described as bound states of two mesons and therefore depend on their interaction, are suppressed, and second, that Regge phenomenology is accurately described. According to Regge theory, the leading contributions to meson and gluon interactions can be described by tree diagrams. In large-N_C QCD, this fact is evident because of the one-particle nature of the resonances; loop diagrams would necessarily be described by two-particle resonances, which are down orders in N_C because they contain internal quark loops.

One relevant consequence of large-N_C QCD is the Hagedorn spectrum[43]. It is easy to observe that the number of mesons diverges as $N_C \rightarrow \infty$, so it is interesting to ask what form this infinite spectrum will take. As Hagedorn concluded, this form is

$$\rho(m) = f(m)e^{m/T_H}. \tag{1.23}$$

This spectrum was first determined phenomenologically from $p - p$ and $\pi - p$

scattering[43, 44], and later gained a more analytical basis with the development of the idea of hadronic strings[45, 46, 47], the formulation of which is one of the many models supported by a large-N_C framework, several of which will be discussed below. Recent data has continued to fit well with the Hagedorn formulation[48].

1.2.3.2   The Nambu-Jona-Lasinio Model

The Nambu-Jona-Lasinio model[49, 50] was originally formulated in the pre-QCD era, but afterwards, has served as a useful simple model for QCD at medium energies, with quarks replacing nucleons as the fundamental degrees of freedom. A detailed review can be found in Ref. [20]. It is constructed as a simple model with quark degrees of freedom. In spite of its simplicity, the NJL model has enduring utility, at least as a pedagogical model, because it is constructed to naturally obey the observed symmetries of QCD. One of the most important of these symmetries is chiral symmetry and its dynamical breaking, which results in constituent quark masses much larger than bare quark masses. As a consequence of this, it has other desirable features such as its ability to reproduce the Goldberger-Treiman and Gell-Mann-Oakes-Renner relation. The simplicity of the NJL model comes at a price, however. One drawback is that the point-like quark interaction leads to a non-renormalizable theory. Thus, all NJL calculations must be done within a specified regularization scheme. Another important limitation is that the NJL model for quarks does not reproduce confinement; this difficulty may or may not be important at energy scales below the perturbative regime.

As with all models describing the intermediate regime between perturbative QCD and low-energy χPT, the NJL model requires a description of both quarks and mesons and the relationship between these degrees of freedom. The simplest NJL lagrangian, using only two flavors of quarks in the isospin limit can be written

$$\mathcal{L}_{\mathrm{NJL}}^{(1)} = \bar{\psi}i\partial\!\!\!/\psi + G\left[(\bar{\psi}\psi)^2 + (\bar{\psi}i\gamma_5\tau\psi)^2\right] - m_q\bar{\psi}\psi. \tag{1.24}$$

While this form is mathematically more tractable than the actual QCD lagrangian, approximations are still necessary to obtain meaningful results. The standard way to perform an NJL calculation is to invoke a mean-field approximation. This is not justified for general N_C; however, as will be discussed below, it becomes exact at large N_C. In this approach, higher-dimensional operators are reduced to linear operators by replacing fields by their mean values. Approximate values for the field are then determined using the effective action approach, treating the field as a small perturbation about its classical value. The quark self-energy in the mean-field approximation can be written as

$$\Sigma = 2G\left[\mathrm{Tr}iS(x,x) - iS(x,x)\right] + 2G(i\gamma_5\tau)\mathrm{Tr}\left\{iS(x,x)i\gamma_5\tau\right\} - 2G(i\gamma_5\tau)iS(x,x)(i\gamma_5\tau),$$

$$\tag{1.25}$$

where the pseudoscalar part of the Hartree term will disappear because it involves the trace of a single γ matrix. Diagrammatically, this is equivalent to the diagrams in Fig. 1.3(a). This approximation is only valid if it is self-consistent; that is, the internal propagator satisfies the same equation. This self-consistency condition requires that the propagator satisfy the equation of motion

$$\left[i\partial\!\!\!/_x - \Sigma\right]S(x,x') = \delta^{(4)}(x-x'), \tag{1.26}$$

26

where Σ is the self-energy from above, which leads to a single consistency condition. The consistency condition corresponds to the implicit inclusion of all cactus diagrams, as per Fig. 1.3(b). Because Σ is independent of x amd x', it can be identified as the mass of the particles in the system, m^*.

Curiously, this expansion is equivalent to the large-N_C expansion. To see this, one must examine the N_C dependence of the NJL coupling constant, G. A quark-antiquark interaction in the NJL model must have a QCD analogue, as depicted in Fig. 1.3(c). The overall N_C counting of the QCD diagram is $1/N_C$, which, by the NJL diagram, requires the NJL coupling to scale as $G \propto 1/N_C$. Then each bubble adding to the cactus diagram adds a factor of $1/N_C$ from the interaction vertex and a factor of N_C from the fermion trace, so all cactus diagrams are of the same order. Attaching an extra loop through more than one interaction point will always produce a diagram lower order in N_C, as each extra vertex would introduce a factor of $1/N_C$. Using this justification, only the Hartree term contributes to the self-energy, as it contains the trace which leads to the extra factor of N_C; the Fock term is one order in N_C suppressed.

The effective mass for the fermion using the self-consistency, or "gap," equation is[20]

$$m^* = m_0 + 2iG \left[N_C N_f + \frac{1}{2} \right] \int \frac{d^4 p}{(2\pi)^4} tr \frac{\slashed{p} + m^*}{p^2 - m^{*2}}, \qquad (1.27)$$

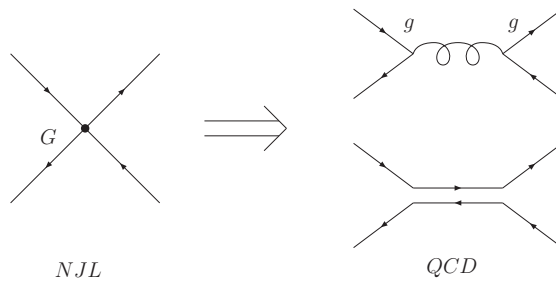which has made use of the self-consistent propagator

$$S(p) = \frac{\slashed{p} + m^*}{p^2 - m^{*2}}. \qquad (1.28)$$

Since the NJL model is to be used at medium energies, however, both quark

(a) fermion self-energy

(b) a cactus diagram

NJL $\implies$ QCD

(c) NJL equivalence with QCD
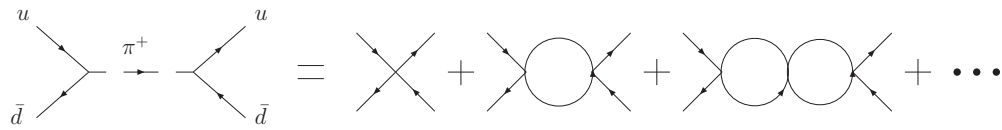
(d) Schematic diagram of quarks interacting with pion

(e) Current to create a pion

Figure 1.3: NJL diagrams

and pion degrees of freedom are of interest. Once the fermion mass has been established, then, it is important to ask how the pion degrees of freedom behave. The pion mass is fairly straightforward to compute under the approximation regime already outlined. Because calculations take place in the mean field approximation, pion fields are taken to be non-interacting, and so a pion can be represented as in Fig. 1.3(d). With the quark interactions of the NJL model, the diagram of Fig. 1.3(d) can then be written[20]

$$
\begin{aligned}
iU_{ij}(k^2) &= (i\gamma_5)T_i\left[2iG + 2iG\left(\frac{1}{i}\Pi_{ps}(k^2)\right)2iG + 2iG\left(\frac{1}{i}\Pi_{ps}(k^2)\right)2iG\left(\frac{1}{i}\Pi_{ps}(k^2)\right)2iG\right. \\
&\quad \left. + \ldots\right](i\gamma_5)T_j \\
&= (i\gamma_5)T_i\left[\frac{2iG}{1 - 2G\Pi_{ps}(k^2)}\right](i\gamma_5)T_j,
\end{aligned}
$$

(1.29)

where the polarization insertion is

$$
\frac{1}{i}\Pi_{ps}(k^2) = -\int\frac{d^4p}{(2\pi)^4}\mathrm{Tr}\,i\gamma_5 T_i iS(p + \frac{1}{2}k)i\gamma_5 T_j iS(p - \frac{1}{2}k).
$$

(1.30)

Given the propagator for the pion, the pion masses can be calculated as the poles of the propagator, or the zeros of its denominator. Thus, the solution to the equation

$$
1 - 2G\Pi_{ps}(k^2) = 0
$$

(1.31)

yields the pion mass. Similarly, the coupling between quarks and pions, $g_{\pi qq}$, can be extracted as the residue of the same pole from eqn. (1.29) as

$$
g_{\pi qq}^2 = \left(\frac{\partial\Pi_{ps}}{\partial k^2}\right)\Bigg|_{k^2=m_\pi^2},
$$

(1.32)

29

and, using the explicit form for Π_{ij} in eqn. (1.30),

$$\frac{1}{g_{\pi qq}^2} = -4iN_C I(0),$$

(1.33)

which will depend on the regularization scheme.

The pions (pseudoscalar modes) should have zero mass in the chiral limit, when the quark mass $m_0 = 0$, which allows them to be identified as Goldstone bosons. To demonstrate this, an explicit expression for m_π can be found from the above expression (in the large-N_C limit), yielding

$$m_\pi^2 = -\frac{m_0}{m^*} \frac{1}{4iGN_C N_f I\left(m_\pi^2\right)}$$

$$I\left(k^2\right) = \int \frac{d^4 p}{(2\pi)^4} \frac{1}{\left[\left(p + \frac{1}{2}k\right)^2 - m^{*2}\right]\left[\left(p - \frac{1}{2}k\right)^2 - m^{*2}\right]}.$$

(1.34)

It is then clear that the pions are massless when $m_0 = 0$.

Other important parameters which relate the properties of the theory to QCD are f_π, the pion decay constant, and Σ, the chiral condensate.

The pion decay constant can be measured using the vacuum to one-pion and axial-vector current matrix element[20] as in Fig. 1.3(e). When this diagram is computed, it is related back to the quark coupling via

$$ik_\mu f_\pi = N_C g_{\pi qq} 4m^* k_\mu I\left(k^2\right).$$

(1.35)

The regularization-independent pion decay constant is then

$$f_\pi^2 = -4iN_C m^{*2} I(0).$$

(1.36)

The relationship between f_π and $g_{\pi qq}$ quickly yields the Goldberger-Treiman relation[51]

$$f_\pi^2 g_{\pi qq}^2 = m^{*2}.$$

(1.37)

The final parameter of interest, Σ, will lead to the Gell-Mann-Oakes-Renner(GMOR) relation[52]. It can be calculated from the scalar number density (in the isospin limit) as

$$\Sigma = \frac{1}{2} \left(\langle \bar{u}u \rangle + \langle \bar{d}d \rangle \right) = -\frac{i}{2} \mathrm{Tr} S(x, x). \tag{1.38}$$

Since $S(x, x) = \int \frac{d^4 p}{(2\pi)^4} S(p)$, the integral in eqn. (1.27) can be rewritten in terms of the chiral condensate, yielding

$$m^* = m_0 - 2G N_f \Sigma, \tag{1.39}$$

and so, combining this result with Eqns. (1.34) and (1.36), the GMOR relation is recovered with

$$m_\pi^2 f_\pi^2 = -2m_0 \Sigma, \tag{1.40}$$

with $m_0 = \frac{1}{2}(m_u + m_d)$ as the quark mass in the isospin limit.

The NJL model, then, is a simple model describing quarks and mesons at medium energies, and is able to reproduce some of the most salient features of QCD at these energies. In any usage of this model, its troubling features cannot be forgotten: it is non-renormalizable and non-confining. However, while the NJL model will not necessarily generate reliable quantitative predictions, it may be of use as an important first step in understanding the qualitative behavior of QCD in a regime where few useful tools exist.

1.3 The QCD vacuum

QCD can be analyzed using different methods in several energy regimes of interest. The relevant energy regime is determined not only by the kinetic energy

and rest mass of the particles under consideration, but can also be imposed by external conditions. To fully analyze the effects of these external conditions, it is important to ask what the key quantities are in describing the state of the system. After analyzing the most basic quantities of QCD (m_π,F_π,Λ_{QCD},etc.), there are several aspects of the theory that can be explored. One is to try to determine the phenomenology of particles in QCD–hadrons at low energy, quarks and gluons at high energy. However, in addition to analyzing how individual particles will interact, it is instructive to study the vacuum itself. As in all quantum field theories, in QCD, the vacuum is non-trivial; particles are always being created and destroyed, and this effect can have real consequences.

In any physical system, the state of the vacuum is characterized by a "phase," with states sharing qualitative behaviors said to be in the same phase. In particular, systems with different symmetries must be in different phases. Measuring the properties of the vacuum under various conditions will help determine the phase of the system. Specifically, quantities which characterize a particular phase transition are called "order parameters" for that transition. *First order* transitions are characterized by a discontinuous change in the order parameter. *Second order* transitions are characterized by a continuous change in the order parameter with a divergent derivative. *Crossover* regions are not properly phase transitions, and the phases which they differentiate, although qualitatively different, will not be discontinuously separated. It can nonetheless be useful to distinguish a crossover point as the point where the derivative of an order parameter is maximized.

One important property of the QCD vacuum is the chiral condensate, defined

in eqn. (1.8). A nonzero value for the chiral condensate is present in the hadronic phase in the absence of any external parameters, but it must go to zero where QCD is perturbative, such as in a high temperature phase. In order to cross into such a regime, then, it will be necessary for some form of phase transition to take place. Thus, the chiral condensate provides a very useful tool which can be used to probe the phase structure of QCD. More complex phase structure will require additional tools, but the chiral condensate is an important first step.

The value of the chiral condensate and other parameters will determine the structure of the QCD vacuum, but in order to vary them and thus the phase, some form of external conditions must be imposed. The most traditional external conditions to examine are temperature and density (or chemical potential). This analysis leads to the familiar QCD phase diagram. In addition, one can probe QCD in an external electromagnetic field, which is the focus of this thesis.

1.3.1 Temperature and density: The QCD phase diagram

The study of the effects of temperature and density on QCD has led to a rich structure for the QCD phase diagram, as seen in Fig. 1.3.1. One of the simplest features is the necessity for a chiral phase transition and for a hadronic phase transition. At high energy scales, including temperature and density, QCD should be in a perturbative regime. This regime is characterized by a sea of quarks and gluons with a vanishing chiral condensate[53], called the *quark-gluon plasma* (QGP)[54]. At low temperatures, QCD is dominated by hadronic interactions, and the chiral
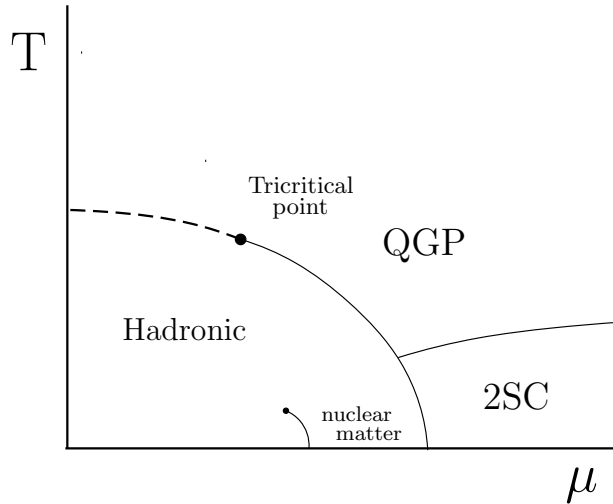
Figure 1.4: The QCD phase diagram: shows the structure of QCD phase transitions at $m_u = m_d \ll m_s$, composed the QGP (Quark-Gluon Plasma), Hadronic phase, nuclear matter phase, and the 2SC (Color superconducting) phase[1]

condensate is observed to have a finite value. There must therefore be a phase transition between these two regimes; in theory, the hadronic phase transition and the chiral phase transition could occur at different temperatures and densities, but they have been observed to be almost exactly coincident[55]. The exact nature and location of this phase transition, as well as the properties of the high-temperature phase, are still under investigation[56]. Currently, the data point to there being a crossover point at zero density and finite temperature, but that at the QCD tricritical point[57, 58, 59, 60, 61, 62], it becomes a first order transition.

Lattice QCD is an effective method for making theoretical predictions at finite temperatures not large enough to be perturbative, but at nonzero μ_B, numerical analysis using lattice methods is extremely problematic, due to the notorious

"Fermion sign-problem"[63]. At finite chemical potential, the fermion action in the lattice formulation becomes imaginary, which results in large complex phases which are problematic in numerical calculation. It is possible to get approximate answers for very small μ_B, but for large μ_B, models are still the only way to obtain theoretical predictions.

Thus, the structure of the phase diagram of QCD is roughly determined by the models as discussed above, with a few caveats. At high temperature the coupling is small, but experimental observations point to the QGP being strongly coupled[64, 65]. Various models and methods of resummation within the QGP have been employed[66], including models such as NJL[67, 57] and effective field theories[68] which are used in other energy regimes, but this is still an open area of investigation. At high densities or μ_B, the system would similarly be expected to be perturbative. However, because the interaction between quarks of different colors is attractive, at high densities diquark condensates form, similar to the formation of Cooper pairs in condensed matter physics[69, 70]. This phenomenon, *color superconductivity* (2SC), has proven key in understanding QCD at high densities[71, 72, 73, 74].

A more detailed discussion of the features of the QCD phase diagram can be found in Ref. [1].

1.3.2 Electromagnetic fields

The effects of electromagnetic fields on QCD are less well-studied than those of temperature and chemical potential. Arguably, regions of finite temperature and chemical potential are more common than those of high electromagnetic field strength, but nonetheless, there are some situations where finite electromagnetic fields can be of interest in QCD, and some curious phenomena arise due to these fields which are not evident elsewhere. On one level, quarks and hadronic matter are minimally coupled to electromagnetism, and their interaction cross sections are naturally affected by electromagnetic fields. On the other hand, the scales at which QCD and QED become perturbative are entirely different, and so it is not possible to perform a perturbative expansion in both couplings. The effect of QED on QCD, in general, will involve an infinite number of insertions of the electromagnetic field. This problem can be solved using the Schwinger proper-time formalism[75], which is used to calculate the exact propagator for any particle in a constant magnetic field.

Using this propagator, the effects of electric and magnetic fields on QCD can be explored in a variety of energy regimes. The chiral condensate is an obvious parameter to examine, as it is the order parameter for chiral symmetry breaking. Using the NJL model and the Schwinger propagator[20, 76], one sees that a magnetic field leads to an enhancement of chiral symmetry breaking, and the electric field leads to a restoration of chiral symmetry. Unfortunately, the electric field also leads to another curious effect in all systems, which is that real pairs of particles can be created out of the vacuum and propagate.

Thus, while it might be possible to plot out the phases of QCD in electromagnetic fields, the diagram would be rather boring. The magnetic field induces a shift away from the known QCD phase transition. The electric field brings the system closer to a phase transition, but the effects of pair production create vacuum instability and it is unclear whether it is possible to sustain such a state.

Physically, electromagnetic fields powerful enough to have a measurable effect on QCD are rare. Magnetars, a type of neutron star[77], the source of the most powerful magnetic fields in nature, have fields that do not exceed $eH \propto (0.02m_\pi)^2$, far below the levels which might affect QCD. Particle accelerators, the source for much of the data in the traditional probes of temperature and pressure, can do better, with some recent experiments at RHIC yielding fields as large as $5.3m_\pi^2$[78, 79, 80], but the energy of the electromagnetic fields in such experiments still does not compare to the energy of the particles themselves.

In addition to affecting the scalar quantities in the vacuum such as the chiral condensate, an externally imposed electromagnetic field is essentially directional. Thus, the vacuum itself will be directionally dependent, and several vectorial quantities can be nonzero. One of these is the magnetization, calculated as

$$\mathbf{M} = \mathbf{B} - \mathbf{H} = \frac{\delta S_{eff}^{matter}}{\delta \mathbf{B}}. \tag{1.41}$$

Finding the magnetization will also help elucidate the effects of a magnetic field on the QCD vacuum.

Chapter 2

External Electromagnetic field at Low-to-Medium field strength

Electromagnetic fields corresponding to low-to-medium energies in QCD are arguably the most physically interesting, but their effects are also more difficult to calculate from first principles than interactions at higher energies. In trying to perform these calculations, the Schwinger propagator for a particle in an electromagnetic field is an important tool which is applicable very generally, but the regime in which a calculation takes place will determine how the Schwinger propagator is used. At low field strengths, the relevant degrees of freedom are the pions, and the relevant calculational scheme is chiral perturbation theory. At intermediate fields strengths, other degrees of freedom begin to be relevant, and some sort of model, such as the NJL model, must be employed until reliable lattice calculations can be obtained. At high energies, the calculations simplify, as perturbative QCD becomes applicable.

Simplicity of calculation is not the only concern. The usefulness of the calculation must also be taken into account. Calculations at energies which are not easily physically achievable are not necessarily irrelevant, as they must yield interesting insights, but experimentally verifiable results are certainly more compelling. QCD becomes perturbative only in certain limited regimes. The largest naturally-occurring magnetic fields are found within magnetars[81], with magnitudes of up

to 10^{11} Tesla. Unfortunately, these maximal magnetic fields are only equivalent to $B \propto (0.02m_\pi)^2$, far below the scale of perturbative QCD. It is therefore desirable to find results within these low-to-medium energy regimes.

This chapter will discuss the derivation of Schwinger's proper time formalism, then proceed to the effects of an electromagnetic field in QCD using the NJL model, chiral perturbation theory for $m_\pi = 0$, and chiral perturbation theory for finite m_π.

2.1 Schwinger's Proper-Time formalism

In 1951, Schwinger proposed the proper time formalism, to solve for the propagator of any charged particle in an electromagnetic field due to its minimal electromagnetic coupling. He found that if one neglected back-reaction, it is possible to calculate a modified propagator for both charged fermions and bosons in the presence of static external fields. The advantage of such an approach is that the modified propagator can be used to account for the effects of minimal coupling in a variety of scenarios, including perturbative QCD, models, and even χPT, which includes additional electromagnetic interactions that can be accounted for separately.

The free propagator for a fermion of mass m minimally coupled to an electromagnetic field A_μ can be written

$$[i\slashed{\partial} - q\slashed{A} - m]\, G(x, x') = \delta(x - x'). \tag{2.1}$$

Defining the operator

$$\Pi_\mu = p_\mu + qA_\mu, \tag{2.2}$$

the equation for the propagator can be symbolically inverted, yielding

$$G = \frac{1}{\not{\Pi} + m}.$$ (2.3)

This can be represented alternatively by introducing a dummy integration variable s, so instead can be written

$$G = i \int_0^\infty ds\, e^{-i(\not{\Pi} - m)s} = i \int_0^\infty (-\not{\Pi} + m) e^{-i(m^2 - (\not{\Pi})^2)s}.$$ (2.4)

It is useful to make the transformation $s \to -is$, which results in an exponential suppression of the infinite integral and a finite result in some situations.

In the case of a constant pure magnetic field in the z direction, this propagator is, for fermions,

$$\begin{aligned} G_{ij}^{(H)}(p) = & - \delta_{ij} \int_0^\infty \frac{ds}{\cosh eHs} \exp\left[-s\left(m_q^2 + p_\parallel^2 + \frac{p_\perp^2}{eHs\coth(eHs)}\right)\right] \\ & \times \left([\cosh(eHs) - i\gamma_1\gamma_2 \sinh(eHs)]\left[\not{p}_\parallel - m\right] + \frac{\not{p}_\perp}{\cosh(eHs)}\right), \end{aligned}$$ (2.5)

and for bosons,

$$D^H(k) = \int_0^\infty \frac{ds}{\cosh(eHs)} e^{-s\left(k_\parallel^2 + k_\perp^2 \frac{\tanh eHs}{eHs} + M^2\right)},$$ (2.6)

where $k_\parallel^2 = k_3^2 + k_4^2$ and $k_\perp^2 = k_1^2 + k_2^2$, and s is the unphysical proper time variable introduced by Schwinger.

The case of a pure electric field is similar mathematically, except that $H \to iE$. From this, Schwinger was able to derive an important consequence of the shift in the propagator. The change to an electric field introduces an imaginary part to the propagator and therefore to the vacuum energy. This vacuum energy in the presence of an electric field can be written

$$W = \frac{1}{2}E^2 - \frac{1}{8\pi^2} \int_0^\infty \frac{ds}{s^3} e^{-m^2 s} \left[eEs \cot eEs - 1 + \frac{1}{3}(eEs)^2\right].$$ (2.7)

40

The singularities along the path of integration, due to $\cot eEs$, can be interpreted as an imaginary part of the integral by assuming that the path of integration lies infinitesimally above the real axis. With a simple quantum mechanical interpretation of the vacuum, where its wave function has a phase e^{iW}, the vacuum persistence probability can be extracted from the vacuum energy as

$$\left| e^{iW} \right|^2 = e^{-2\mathrm{Im}W}. \tag{2.8}$$

Thus, an imaginary part in the vacuum energy will result in a shift away from this vacuum. Schwinger interpreted the physical mechanism for the breakdown of the vacuum as pair creation. That is, in quantum field theory, virtual particle and anti-particle pairs are constantly being created. Using a rough physical picture, in the absence of an electric field, these virtual pairs recombine without incident. However, in the presence of an electric field, when this particle-antiparticle pair is created with an orientation which tends to pull the particles apart, there will be a negative potential energy for the state proportional to the separation of the particles. If the potential energy of this state is larger than the masses of the particles, then the state can survive and the particles will be pulled apart. The probability to create a particle pair is exponentially suppressed by its separation, and since the separation required is proportional to the masses of the particles, the probability to create this particle pair will be exponentially suppressed by the mass of the particles.

This pair creation, the *Schwinger mechanism*, has gained wide acceptance in the time since Schwinger proposed it. There has been some discussion as to the exact relation between the vacuum persistence and the pair creation rate [82, 83, 84], but it

is well-established that there is some vacuum instability due in part to pair creation. Because it describes an instability, there is an inherent limitation to the time scales over which the Schwinger mechanism can be valid. There are two aspects of this dynamic nature. The first is back-reaction in the electric field[85, 86, 87, 88, 89], where the newly-created pairs generate a current and an electric field, which leads eventually to plasma oscillations. This mechanism requires that enough pairs be created that their effects become comparable to the magnitude of the field.

Another effect, though theoretically might be avoided, results from the ultimately finite nature of any real system[90]. First, it is important to note that the Schwinger mechanism is highly dependent upon the boundary conditions of the system–i.e., that the system starts in a pure vacuum. The mathematical interpretation of singularities in the propagator as positive imaginary parts is dependent upon this physical necessity, and is not accurate when the vacuum state is more complex. The physical situation described by Ref. [90] illustrates this fact. Rather than describing a system in a pure vacuum with an electric field which is constant everywhere, it is possible to examine an ideal parallel-plate capacitor, with a large separation and field. In this case, there is an imbalance in states, where filled negative energy states on one side of the capacitor correspond to empty positive energy states on the other side. Pair creation will occur as these states propagate from one side to the other; however, once all states on both sides of the capacitor are equalized, pair creation will cease[83, 90].

In many of the cases discussed below, the imaginary part in the condensate is taken to be a signal of pair creation, with the magnitude of the imaginary part

taken to roughly correspond to the importance of the pair creation. Only in the very specific case of the imaginary part of the vacuum energy shift does this imaginary part exactly correspond to pair creation, however, the singularities in other observables are related and can be used as a qualitative measure.

2.2 Electromagnetism in the NJL model

Because the NJL model was one of the earliest attempts at describing the strong force and later QCD at medium energies, there is extensive work describing the effects of the electromagnetic field using the NJL model and other related models. The NJL model has many drawbacks. However, the chiral condensate and chiral symmetry breaking are closely related to the symmetry of the lagrangian and arguably not dependent on confinement, and are therefore quantities which are natural to study in this model. Klevansky and Lemmer[76] incorporated the electromagnetic field into the NJL model through minimal coupling, and then used Schwinger's propagator to include the effect of the action to all orders in the field strength. This discussion follows their work closely as discussed in Ref. [20].

The NJL lagrangian can be minimally coupled to electromagnetism by introducing the four-potential A_μ, with the result that

$$\mathcal{L}_{NJL+EM} = \mathcal{L}_{NJL} - q\bar{\psi}\gamma_\mu A^\mu \psi - \frac{1}{4}F^2, \tag{2.9}$$

where $\mathcal{L}_{NJL}$ has been defined in Eq. (1.24). Then the self-consistent propagator from Eq. (1.26) must satisfy a new relation,

$$[i\slashed{\partial}_x - e\slashed{A}(x) - \Sigma(x)]\, S_A(x, x') = \delta^{(4)}(x - x'), \tag{2.10}$$

where $S_A(x, x)$ can be related back to the fermion self energy as $\Sigma(x) = 2igtrS_A(x, x)$, and

$$q_F = \frac{1}{2}e\left(\tau_f + \frac{1}{3}\right). \tag{2.11}$$

Without electromagnetism, in a homogenous system, Σ is independent of x and can be interpreted to be the mass. This is not necessarily the case when an electromagnetic field is present, but if the field is constant, then the self-energy will be constant and can still be interpreted as the dynamically-generated mass, $\Sigma = m^*$. The procedure for obtaining the gap equation is very similar to the case without electromagnetism, except that the pseudoscalar vertex cannot be ignored in the Hartree term, as the A_μ term contributes another γ matrix.

Neglecting the Fock term, which is smaller by an order of N_C, the equation for the fermion self-energy can be written

$$\Sigma = m^* = m_0 + 2iG\text{Tr}S(x, x) + 2iG(i\gamma_5)\tau\text{Tr}\left\{i\gamma_5 S(x, x)\tau\right\}. \tag{2.12}$$

As promised, it is possible to solve Eq. (2.10) using Schwinger's proper time formalism, since Σ is x-independent, though unknown. Using the generalized fermion propagator, the self-energy for a fermion of flavor f can be written as

$$
\Sigma^f = m_0 - \frac{GN_C}{2\pi^2}\Sigma^f\left(\sum_g\left[\int_0^\infty \frac{ds}{s^2}e^{-M^2s}q_gF's\cot(q_gF's)q_gF''s\coth(q_gF''s)\right]\right.
$$
$$
\left. + i\gamma_5\tau_f\frac{F'F''}{M^2}(q_u^2 - q_d^2)\right), \tag{2.13}
$$

where F' and F'' are related to the eigenvalues of the Lorentz invariants $\mathcal{F} =$

$\frac{1}{2}\left(\mathbf{H}^2 - \mathbf{E}^2\right)$ and $\mathcal{G} = \mathbf{E} \cdot \mathbf{H}$ as

$$iF' = \frac{i}{\sqrt{2}}\left[(\mathcal{F} + i\mathcal{G})^{\frac{1}{2}} - (\mathcal{F} - i\mathcal{G})^{\frac{1}{2}}\right]$$

$$F'' = \frac{i}{\sqrt{2}}\left[(\mathcal{F} + i\mathcal{G})^{\frac{1}{2}} + (\mathcal{F} - i\mathcal{G})^{\frac{1}{2}}\right].$$

(2.14)

In the frame where $E||H$ (which can always be chosen by Lorentz invariance), these can be written more simply as $F' = iE$ and $F'' = iH$. Separating the divergent portion of the integral from the non-divergent portion, and neglecting the pseudoscalar term, which is irrelevant in the case where $F' = 0$ or $F'' = 0$ (a pure electric or magnetic field), the dynamically generated mass becomes

$$m^* = m_0 + \frac{GN_C m}{2\pi^2}\left[\sum_f \int_0^\infty \frac{ds}{s^2} e^{-m^{*2}s}\left[q_f F's \cot(q_f F's) q_f F''s \coth(q_f F''s) - 1\right]\right.$$
$$\left. + \sum_f \int_0^\infty \frac{ds}{s^2} e^{-m^{*2}s}\right].$$

(2.15)

The first piece is finite for $s \to 0$; only the second piece contains divergences. As is always the case with Schwinger propagators, there will be an imaginary piece in the integral which will contribute to the non-persistence of the vacuum. A large imaginary component may cast doubt on the validity of the answer, but otherwise, it is the principal value of this integral that is of interest. The NJL model always results in divergent integrals, and so NJL quantities must be regularized. In this case, because the external fields prevent an arbitrary cut-off, Pauli-Villars regularization[91] should be used, which involves coupling the interaction to some number of arbitrary massive fields. This corresponds to rewriting the divergent portion of the integral

45

$(I_D(m^2))$ as

$$I_D(m^2) = \lim_{\rho \to 0} \sum_a C_a \int_\rho^\infty \frac{ds}{s^2} e^{-M_a^2 s}. \tag{2.16}$$

The conditions $\sum C_a M_a^2 = 0$ and $\sum C_a = 0$ are imposed, which force the divergences to cancel, leaving only logarithms in the masses of the auxiliary fields and the original mass. This application results in

$$\begin{aligned} I_D(m^2) &= \sum_a C_a M_a^2 \log \frac{M_a^2}{m^2}. \\ &= \Lambda^2 \left[\left(2 + \frac{m^2}{\Lambda^2} \right) \log \left(1 + 2\frac{\Lambda^2}{m^2} \right) - 2 \left(1 + \frac{m^2}{\Lambda^2} \right) \log \left(1 + \frac{\Lambda^2}{m^2} \right) \right], \end{aligned} \tag{2.17}$$

where the masses of the auxiliary fields are chosen as functions of m and an arbitrary scale Λ.

Further calculation requires choosing particular values for F' and F''. Klevansky[20] chooses to first examine the electric field, because it results in chiral symmetry restoration, despite the difficulties of a nonzero imaginary portion of the integral. The equation can then be rewritten as

$$\frac{2\pi^2}{GN_C} \left[1 - \frac{m_0}{m^*} \right] = N_f I_D(m^2) + \sum_f q_f E \mathrm{Re} I_{EM}(im^2/2q_f E), \tag{2.18}$$

where I_{EM} stems from the principle value of the divergent integral as

$$\int_0^\infty] \frac{ds}{s^2} e^{-m^2 s} [q_f E s \cot q_f E s - 1] = q_f E I_{EM}(im^2/2q_f E), \tag{2.19}$$

and can be calculated in closed form as

$$I_{EM}(z) = 2i \left[\left(z - \frac{1}{2} \right) \log z - z \log \Gamma(z) + \frac{1}{2} \log 2\pi \right]. \tag{2.20}$$

A pure electric field can be exchanged for a pure magnetic field by taking $E \to iB$, which are equivalent in the Lorentz invariants $\mathcal{F}$ and $\mathcal{G}$.

The self-consistency equation for m^* cannot in general be solved analytically, but can be plotted numerically. For $m_0 = 0$, it is possible to find a value for m^* which is zero for some E field, leading to chiral symmetry restoration. This critical field strength is[76]

$$qE_C = \frac{2\Lambda'^2}{\pi}\left(1 - \frac{2\pi^2}{GN_C N_f \Lambda'^2}\right),\tag{2.21}$$

where $\Lambda'^2 = 2\Lambda^2 \log 2$. Using $\Lambda = 851$ MeV and $G\Lambda^2 = 2.87$, which correspond to the physical values $f_\pi = 94$ MeV and $\langle \bar{q}q \rangle = (-250 \text{ MeV})^3$ in the absence of an electromagnetic field, Ref. [76] calculates this critical strength to be 0.56 GeV fm^{-1}.

With realistic values for the current quark masses (5.2 MeV), this phase transition due to the electric field is no longer present. And, as discussed, in the case of a magnetic field, the sign in the shift is opposite, so the masses move even further away from the chirally-symmetric phase.

Other models incorporating electromagnetism have found qualitatively similar results[92, 93, 94, 95, 96, 97, 98, 99], and an expansion of this result for small fields finds that the shift in the condensate for a magnetic field can be written

$$\Sigma(H) = \Sigma(0)\left[1 + C\frac{e^2 H^2}{\Sigma^4} + O\left(\frac{e^4 H^4}{\Sigma^8}\right)\right].\tag{2.22}$$

2.3 Electromagnetism in χPT at the chiral limit

Chiral Perturbation theory is model-independent, depending only on the convergence of the chiral expansion and the LECs, so χPT calculations are to some degree more robust than those made with models such as NJL. As discussed in the introduction, it is formally applicable at all energies $p \ll \Lambda_H$. The Schwinger prop-

agator is an exact result, and as such applies at any energy scale. Because χPT is valid in the same regime where QED is valid, it might be fruitful to pursue a perturbative expansion including a finite number of photon insertions. This section will aim to do that; the derivation is based on work originally published in Ref. [100], and follows that work closely.

The chiral condensate will be the probe of choice in this analysis. In the case of a constant electromagnetic field at these energies, there is a convenient shortcut to measuring its value. In the path-integral formalism, the expectation value for an operator can be calculated in the presence of an external source from the functional integral representation. Here, we define

$$Z[m] = e^{-\epsilon_{vac}[m]} = \int \mathcal{D}\psi \mathcal{D}\bar{\psi} \exp\left[i \int d^4x \left(\mathcal{L}[\psi, \bar{\psi}] + m\bar{\psi}\psi\right)\right]. \qquad (2.23)$$

Then the value for the chiral condensate can be calculated as

$$\Sigma = \langle \bar{\psi}\psi \rangle = -\left.\frac{\delta\epsilon_{vac}}{\delta m_u}\right|_{m_u=0}. \qquad (2.24)$$

Using the Gell-Mann-Oakes-Renner relation, $m_\pi^2 f_\pi^2 = -(m_u + m_d)\Sigma$, to convert this derivative in the current quark mass to a derivative in the pion mass yields

$$\Sigma = \frac{\Sigma}{F_\pi^2} \frac{\partial\epsilon_{vac}}{\partial M_\pi}. \qquad (2.25)$$

Past work[101] in χPT has concentrated on the magnetic field; the shift due a pure magnetic field is strictly well defined. The cases of a pure electric field or a mixed field are intrinsically ambiguous due to the imaginary part associated with pair creation.
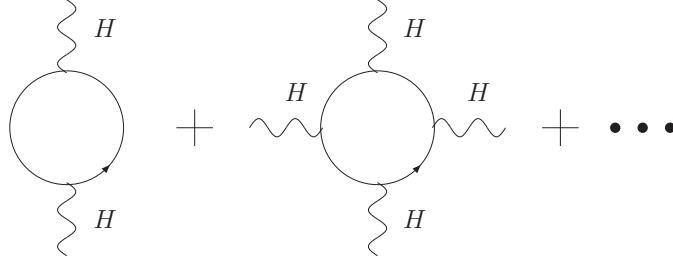
Figure 2.1: Lowest-order diagrams treating an electromagnetic field in χPT with a finite number of insertions

In general, the vacuum energy will be infinite; however, the part related to the electromagnetic field will be finite, and thus a meaningful answer can be extracted. The diagrams used to extract this lowest-order contribution are depicted in Fig. 2.3.

Using this approach, Ref. [101] found the first order shift in the condensate to be

$$\Delta\Sigma^{(2)}(H) = \Sigma\frac{eH}{(4\pi F_\pi)^2}\left(\frac{eH}{6M_\pi^2}\right). \tag{2.26}$$

However, there is a potential difficulty in this approach. In the chiral limit, $m_u = m_d = 0$, the pion mass $m_\pi \to 0$, which would result in Eq. (2.26) diverging. It is worth mentioning that the term "chiral limit" is not absolutely synonymous with $m_\pi = 0$; technically speaking, a system with a finite H field will never be in the chiral limit, because an electromagnetic field will explicitly break chiral symmetry. Nonetheless, we will refer to the situation of $m_\pi = 0$ as the "chiral limit."

Ref. [101] solved the difficulty above using Schwinger's full result for a constant

magnetic field,

$$\epsilon_{vac} = -\frac{1}{(4\pi)^2} \int_0^\infty \frac{ds}{s^3} e^{-M_\pi^2 s} \left[\frac{eHs}{\sinh(eHs)} - 1 \right],$$ (2.27)

which resulted in a well-defined chiral condensate for the limit $m_\pi \to 0$. Taking the derivative with respect to the pion mass and the limit $m_\pi \to 0$ yields

$$\Sigma(H) = \Sigma(0) \left[1 + \frac{eH \ln 2}{(4\pi F_\pi)^2} + \cdots \right].$$ (2.28)

This answer is not only quantitatively different from the answer in Eq. (2.22), but the different parameters appearing in this result demonstrate that they are different expansions altogether. Here, the dependence on eH is linear, whereas in the NJL model it is quadratic. Similarly, the N_C dependence is different; because of the factor of F_π in the denominator (where $F_\pi \propto N_c^{1/2}$), this result is one order in N_C reduced from the previous shift. For very small H fields, the shift derived in χPT will be the leading order term, but as H becomes larger, depending upon N_C, there will be some point where the term of order N_c^0 (as seen for example in the NJL model) becomes dominant. This can be viewed as a case of non-commuting limits, which appear in QCD in many other well-known cases[102, 103, 104, 105, 106]. In such cases, it is important to be unusually careful in choosing which limit to take first. Because χPT contains all possible forms of the interaction by design, it can be expected that higher orders in the chiral expansion would contain terms which shift the chiral condensate in the same way as the NJL model; this will be discussed in Chapt. 3.

In addition to the difficulties due to non-commuting limits, there is another more profound inconsistency with this result. The chiral limit, $M_\pi \to 0$, requires
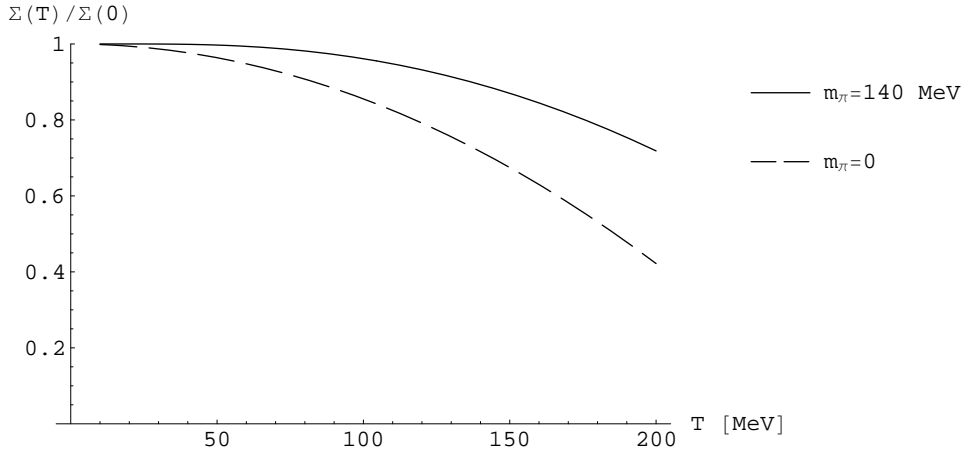
Figure 2.2: Shift in the condensate to one loop plotted as a function of temperature in the chiral limit and with a realistic finite value for m_π.

that M_π be much less than all other scales in the problem. It is of course true that $M_\pi \ll \Lambda_H$, which is a requirement for the chiral expansion, but there is another scale in the problem: $\sqrt{eH}$. This scale must also obey the relation $eH \ll \Lambda_H^2$ in order for the chiral expansion to be valid. Together, these requirements impose a strict hierarchy of scales, $M_\pi^2 \ll eH \ll \Lambda_H^2 (4\pi F_\pi)^2$, which must be fulfilled in order for the analysis of Ref. [101] to hold. The physical values of M_π and F_π are known, and optimistically, $\Lambda_H^2/M_\pi^2 \sim 50$. This leaves a very narrow region of validity in which an H field can meet these requirements, and arguably, it is not possible for an H field to satisfy both conditions simultaneously.

The chiral limit can have similar difficulties in other problems, as well. At finite temperature, the "low-energy theorem" derived from χPT regarding the behavior

of the condensate, taken at the chiral limit, is

$$\frac{\Sigma(T)}{\Sigma(0)} = 1 - \frac{T^2}{8F_\pi^2} - \frac{T^4}{384F_\pi^4} - \cdots \qquad (2.29)$$

Similarly to the case of the magnetic field, this series only converges when there is a strict hierarchy of scales, $m_\pi \ll T \ll T_c \lesssim \Lambda_{QCD}$. Just as with the magnetic field, the possible range of temperature for which this theorem is valid is very narrow. Any temperature large enough for the chiral limit to be valid has passed beyond T_c and is well outside the region of validity of χPT. It is still possible to hope that the theorem may still be applicable even when it is not formally valid, but fig. 2.2 shows that this is not the case and that the shift in the condensate for a finite m_π is much different than that expected in the chirally symmetric case.

Given these difficulties, it becomes critical to examine the effects of a finite M_π on the result.

2.4   The effects of a finite M_π

Addressing the case of the chiral condensate in an electromagnetic field for finite M_π (the chiral limit) is desirable because of the doubtful validity of the prior result. A further interesting generalization will be to analyze the effects of a pure electric field or of a mixed field. As discussed previously, both of these situations will lead to an imaginary part in the expression for the condensate, which indicates a fundamental instability in the result due to the creation of particle-antiparticle pairs from the vacuum. Nonetheless, an analysis of the χPT result can provide some guidance as to when this instability proves significant. This section discusses results

originally obtained in Ref.[100], and follows closely the derivations therein.

At lowest-order, pions, the relevant degree of freedom at low energies, are non-interacting. Their interactions with the electromagnetic field occur in the $\mathcal{L}^{(2)}$ lagrangian. As determined by Ref. [101], an interaction vertex reduces the result in powers of eH/m_π^2, which is invalid in the chiral limit. Given the assertion that magnetic fields not much greater than m_π are more realistic for a number of reasons, this might be attractive once the chiral limit has been given up. However, the limit $eH \ll m_\pi^2$ is also unecessarily restrictive, and a more general approach would be to consider the case $m_\pi^2, eH \ll \Lambda_H$, without imposing any additional restrictions on the relationship between m_π^2 and eH. Therefore, it is still advantageous to consider an infinite number of insertions contributing to the result and the Schwinger propagator is necessary.

The first-order vacuum energy in the case of a generalized electromagnetic field was calculated by Schwinger to be[75]

$$\epsilon_{\text{vac}} = \frac{1}{16\pi^2} \int_0^\infty ds s^{-3} e^{-m_\pi^2 s} \left(\frac{(es)^2 \mathcal{G}}{\text{Im}(\cosh esX)} - 1 \right), \qquad (2.30)$$

where $\mathcal{F} = \frac{H^2 - E^2}{2}$ and $\mathcal{G} = \vec{E} \cdot \vec{H}$ and $X = (\mathcal{F} + i\mathcal{G})^{\frac{1}{2}}$.

2.4.1 Constant Magnetic Field

The Schwinger expression for the vacuum energy is complicated, and it turns out, as will be discussed later, that for arbitrary E and H fields, only numerical studies will be possible. In order to proceed to some analytical result, then, it is necessary to choose either a pure magnetic or a pure electric field. Because the

magnetic field does not have the problematic issue of pair creation (and an imaginary component of the integral), it will be the simplest situation to consider first.

In a pure H field, the expression in Eq. (2.30) can be simplified to the result in Eq. (2.27). This result is simplified by Ref. [101] in the chiral limit. Writing the result differently, in order to highlight the differences between the chiral limit and finite m_π, yields

$$
\Delta\Sigma(H) = \frac{\partial\mathcal{L}_{\mathrm{eff}}}{\partial m_u} = \frac{\log(2)\, eH\Sigma(0)}{16\pi^2 F_\pi^2} I_H\left(\frac{m_\pi^2}{eH}\right)
$$
$$
I_H(y) \equiv -\frac{1}{\log(2)} \int_0^\infty \frac{dz}{z^2} e^{-yz}\left[\frac{z}{\sinh(z)} - 1\right] ,
$$
(2.31)

where the parameter y is the dimensionless ratio m_π^2/eH. $I_H(y)$ is defined in such a way that the value of the integral in the chiral limit yields $I_H(0) = 1$, returning the prior result. This is the one-loop order χPT result which makes no assumptions about the ratio m_π^2/eH and is therefore able to incorporate a finite m_π. It is then possible to analyze how accurate the prior result, derived in the chiral limit, is in describing the result for finite m_π.

This expression includes the subtraction of an infinite term equal to $\epsilon_{\mathrm{vac}}(H = 0)$, to yield a finite contribution for the shift due to the magnetic field. It is possible to have tree-level, inherently finite, diagrams which contribute to the vacuum energy, but because of the nature of the chiral expansion, these terms do not contribute at lowest order. Any tree diagram would require a vertex with two powers of the magnetic field, $(eH)^2$, and a power of the mass squared, m_π^2, in order to result in a contribution for non-zero H and a non-zero result in the variation with respect to the pion mass. Such a term would have a minimum power of $\mathcal{O}(p^6)$, and therefore

does not contribute at $\mathcal{O}(p^4)$. These terms are still potentially intersting, as they are also closer to the form of the NJL result, and will be discussed in Chapt. 3.

Conveniently, it is also possible to derive a closed-form analytic result for this integral using standard mathematics[107]:

$$I_H(y) = \frac{1}{\log 2} \left(\log(2\pi) + y \log \left(\frac{y}{2} \right) - y - 2 \log \Gamma \left(\frac{1+y}{2} \right) \right). \tag{2.32}$$

The comparison of the result in the chiral limit to the result for finite $m_\pi = 140 MeV$, using this analytic expression, is plotted in fig. 2.3. From this plot, it is clear that the convergence to the chiral result is very slow, with a substantial difference even as high as $eH/m_\pi^2 = 30$, where the one-loop expression is still only 85% of the value for $m_\pi = 0$. It is also clear from the plot that even when $eH/m_\pi^2 = 50 \sim \Lambda_H^2/m_\pi^2$, far outside the validity of the chiral expansion, that there are still substantial differences between the $m_\pi = 0$ result and the result for finite m_π. Any value of eH large enough for the $m_\pi = 0$ result to be reasonably close to the more accurate result for finite m_π is so far above the region of validity for the chiral expansion that even higher-order terms are unlikely to make the result credible. However, the generalized low-energy theorem is valid for any relationship between m_π^2 and eH, as long as both are small enough for the chiral expansion to be valid.

2.4.2 Constant Electric Field

Prior analysis in the chiral limit[101] concentrated primarily on the magnetic field; the electric field presents problems due to the imaginary part, but as was done in Ref. [100], it is possible to derive a result for both the real part and imaginary
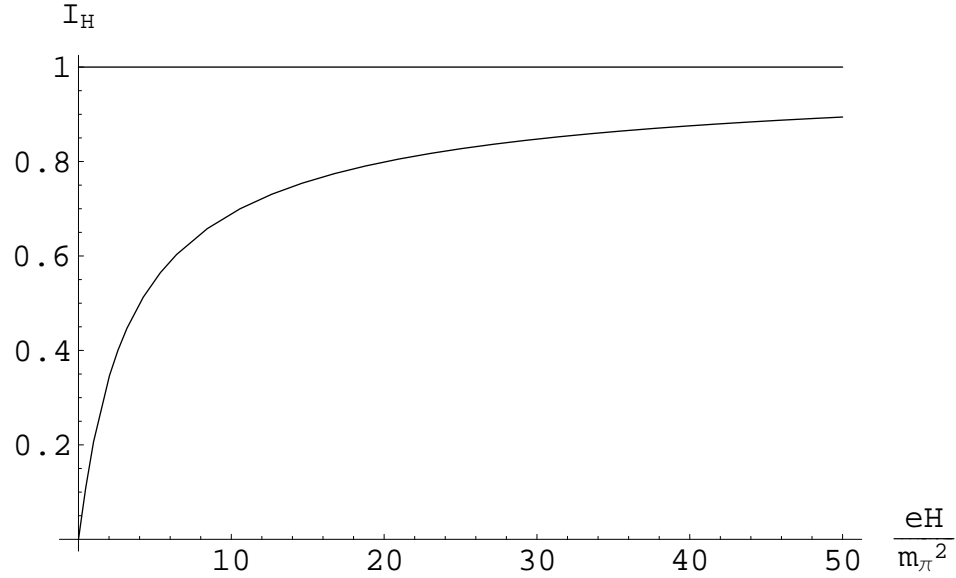
Figure 2.3: Exact expression for the integral representing the shift in the condensate plotted as a function of eH/m_π^2, as compared to the $m_\pi = 0$ value of unity.

part, and the comparison of these quantities can help to understand when the result is sensible. The NJL calculations have addressed the problem of the electric field and derived an expression for the condensate, but this expression consists only of the real part, neglecting the effects of the imaginary part of the result. One interesting aspect of these calculations, as discussed above, is their derivation of a critical electric field which leads to chiral symmetry restoration. To the extent that the imaginary part can somehow be neglected, this is sensible in the NJL model, which, to the extent it is valid at all, should be valid up to the energies of this critical electric field. Even without the imaginary part, however, such a critical electric field is outside the range of validity of χPT, so will not be discussed here.

In general, this imaginary part represents an instability in the state of the

system; the vacuum is not the true ground state. Mathematically, in simple quantum mechanics, the time-evolution operator of the vacuum for a simple quantum mechanical system goes like $e^{i\epsilon_{vac}t}$; for a real vacuum energy for the single vacuum state, this is merely a phase. If the vacuum energy is imaginary, then the state will evolve away from this "vacuum" into another state. For the electric field, this instability can be interpreted to be pair creation. In the NJL model, the degrees of freedom are quarks, so the imaginary part represents the creation of quark pairs from the vacuum; χPT describes the interactions of pions, so the instability in that case represents the creation of charged pion pairs $(\pi^\pm)$ from the vacuum. However, one of the most important issues with the NJL model is its lack of confinement; in that case, the instability in the imaginary part could be argued to be a result of this flaw. However, χPT has no analogous difficulty, so the imaginary part is a physical instability.

Knowing, then, that there are some circumstances under which the shift in the condensate due to the electric field is meaningless, it is important to understand what these circumstances are in the context of χPT. In physical systems, the real and imaginary parts will cause two separate effects: first, the shift in the condensate due to the real part, and second, the creation of $\pi^+ - \pi^-$ pairs due to the imaginary part. If the condensate shift takes place more quickly than the pair creation from the vacuum, then it will be sensible to consider the principal value of the integral alone, without taking into account the imaginary part. If, on the other hand, pair creation takes place on a time scale similar to that of the condensate shift, then it will no longer be reasonable to consider the real part alone; even if the pair creation is not

57

large enough to change the electric field, a system with many free charges is not the same as the vacuum and calculations must be treated in a qualitatively different way. Because it depends on the exponential of the time-evolution operator, the rate scales as $\exp\left(-\frac{\pi m_\pi^2}{eE}\right)$, and is thus exponentially suppressed for eE substantially smaller than m_π. It is certainly the case, then, that in the regime $eE \ll m_\pi^2$ that the instability due to pair creation mechanism is slow and that this instability can be neglected.

Another useful tool is the ratio of the imaginary part to the real part of the shift. This is a rough indicator of whether the effects of the real part or the imaginary part is dominant. While the effects produced by each cannot be directly compared, it is clear that if the imaginary part is on the order of the real part, the instability cannot be neglected in comparison to the shift in the condensate.

The shift due to the electric field will also be calculated to one loop in χPT. While the qualitative situations in the magnetic and the electric field cases are quite different, especially because of the instability discussed above and the reversal of sign, the mathematical method for calculating each is very similar, and both can be derived from Eq. (2.30). The chiral condensate is a Lorentz scalar, so must depend only on Lorentz-invariant quantities. The two unique Lorentz invariants that can be constructed from the electric and magnetic fields are $\mathcal{F} = \frac{1}{2}\left(\mathbf{H}^2 - \mathbf{E}^2\right)$ and $\mathcal{G} = \mathbf{E}\cdot\mathbf{H}$. For either a pure magnetic or a pure electric field, $\mathcal{G} = 0$, and so the answer will only depend on $\mathcal{F}$, which will be positive for a pure magnetic field and negative for a pure electric field. An electric field of E is mathematically equivalent to a magnetic field of $H \to iE$. Formally, it is necessary to make an analytic continuation of the

result for the condensate, but practically, a direct substitution is suitable in this case.

The integrand in Eq. (2.31) depends on the magnetic field through $y = m_\pi^2/eH \to m_\pi^2/ieE = -iy'$. To keep yz real and positive, it is necessary to modify $z \to iz'$. The integral part of the shift in the case of the electric field can then be written

$$I_{H\to iE}(-iy') = -\frac{1}{\log 2}\int_0^\infty (-i)\frac{dz'}{z'^2}e^{-y'z'}\left[\frac{z'}{\sin z'} - 1\right]. \qquad (2.33)$$

Redefining $-iI_E(y) \equiv I_H(-iy')$ to avoid explicit factors of i, the full shift can be written[100]

$$\Delta\Sigma(E) = \Sigma(0)\left[\log(2)\frac{eE}{16\pi^2 F_\pi^2}I_E\left(\frac{m_\pi^2}{eE}\right)\right]$$

$$I_E(y) = -\frac{1}{\log 2}\int_0^\infty \frac{dz}{z^2}e^{-yz}\left[\frac{z}{\sin z} - 1\right]. \qquad (2.34)$$

While the integrand for I_H has no poles, the $\sin(z)$ in the denominator of the I_E integrand results in an infinite number of poles along the axis of integration, leading to an imaginary part of the shift. One caution here is that it is not immediately obvious from this expression how to treat these poles; it is possible to choose an integration path infinitesimally above the axis, below the axis, or to simply choose the principal value. The choice of treatment is dependent upon the physical boundary conditions imposed. The convention used by Schwinger[75], corresponding to the creation of pairs from the vacuum, is the substitution $1/\sin(z) \to 1/(\sin(z) + i\epsilon)$. The shift is then mathematically well-defined. The shift $1/\sin(z) \to 1/(\sin(z) - i\epsilon)$ would correspond to the recombination of pairs in the vacuum, and the principal value would correspond to some steady-state solution. Both of these latter solutions

require pre-existing particles in the vacuum, so the Schwinger choice seems to be the most sensible here, resulting in the instability discussed above. However, this situation deserves some careful examination, and some recent work has shown that the Schwinger mechanism is not necessarily as straightforward as it originally appeared to be[108].

Proceeding with the standard interpretation, then, it is straightforward to find the imaginary part of the integral. There are an infinite number of non-trivial poles along the integration axis, and their residues correspond to the imaginary part of the integral, whereas the real part corresponds to the principal value of the integral. These poles represent the instability mentioned above and will result in the evolution over time from a vacuum which is empty of particles. The principal value part of this integral may be more difficult to obtain.

Practically, there are actually two ways to find a result for this integral: Analytic continuation of the result from Eq. (2.35) and direct evaluation of the principal value and the poles in Eq. (2.34).

The apparently easier way is to analytically continue the closed-form result for the integral. Making the standard choice of branch cut yields for the analytic expression[100]

$$
\begin{aligned}
\mathcal{I}(I_E) =& \frac{1}{\log 2} \log(1 + e^{-\pi y}) \\
\mathcal{R}(I_E) =& \frac{1}{\log 2} \left\{ y \log \left(\frac{y}{2} \right) - y + Cy + 2 \tan^{-1} y \right. \\
& \left. + 2 \sum_{n=1}^{\infty} \left[\tan^{-1} \left(\frac{y}{2n+1} \right) - \frac{y}{2n} \right] \right\}
\end{aligned}
\tag{2.35}
$$

where C is Euler's constant. These expressions result in analytic expressions for the
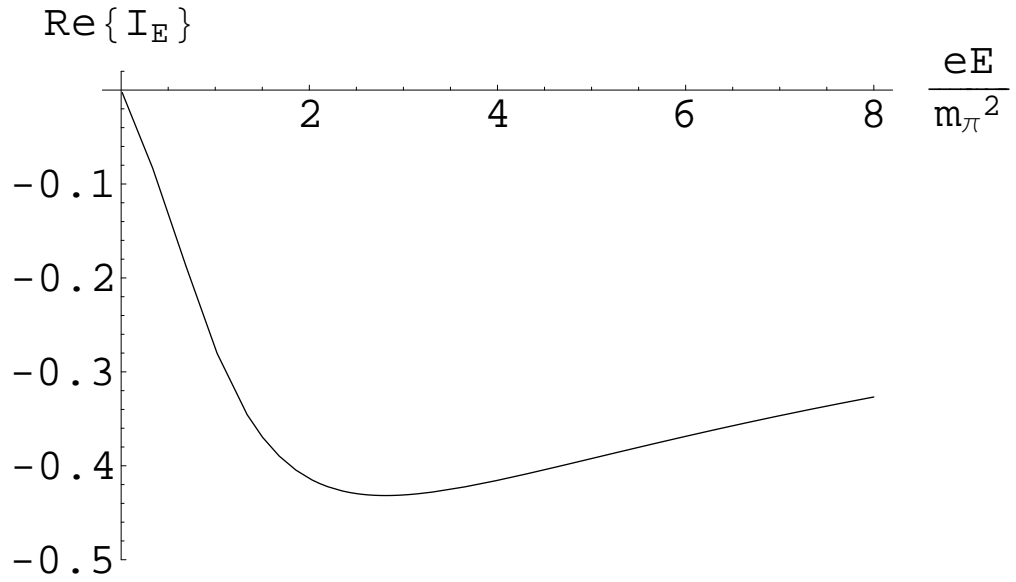
real and imaginary parts of the shift in the case of an electric field. However, because of the analytic continuation, it is not immediately apparent that these expressions include the correct branch cuts of the function.

The next way is to evaluate the integral directly, which is more reliable but also more involved. It is straightforward to find the sum of the poles from the integrand, and as expected it is the same as the imaginary part found in Eq. (2.35). It is also important to compare the principal value to its value in this equation. Unfortunately, this is a bit trickier, as there is no really straightforward way to evaluate the principal value of the integral analytically, due to the singularities in the integration path. However, it is possible to employ a trick to evaluate the integral numerically. New terms can be added to the integrand which have zero principal value, but which exactly cancel the poles, to yield the expression[100]

$$
P(I_E) = \int_0^\infty dz \left\{ \frac{e^{-yz}}{z^2} \left[\frac{z}{\sin(z) + i\epsilon} - 1 \right] \right.
$$
$$
\left. - \sum_{n=1}^\infty \frac{(-1)^{n-1}}{n\pi} e^{-n\pi y} \left(\frac{1}{z - n\pi + i\epsilon} - \frac{1}{z + n\pi + i\epsilon} \right) \right\} .
$$

(2.36)

This extracts the principal value, but is unfortunately still not easy to evaluate analytically. It is nonetheless possible to evaluate this expression numerically, since it is completely real-valued; doing so results in the same answer as in Eq. (2.35), to very high precision.

The values for the real and imaginary parts (identical in both derivations) are plotted in fig. 2.4. As discussed above, the ratio of the imaginary part to the real part dictates the regime of validity for the pricipal value of the result; this ratio is plotted in fig. 2.5.

(a) $Re\{I_E\}$ vs eE/m_π^2
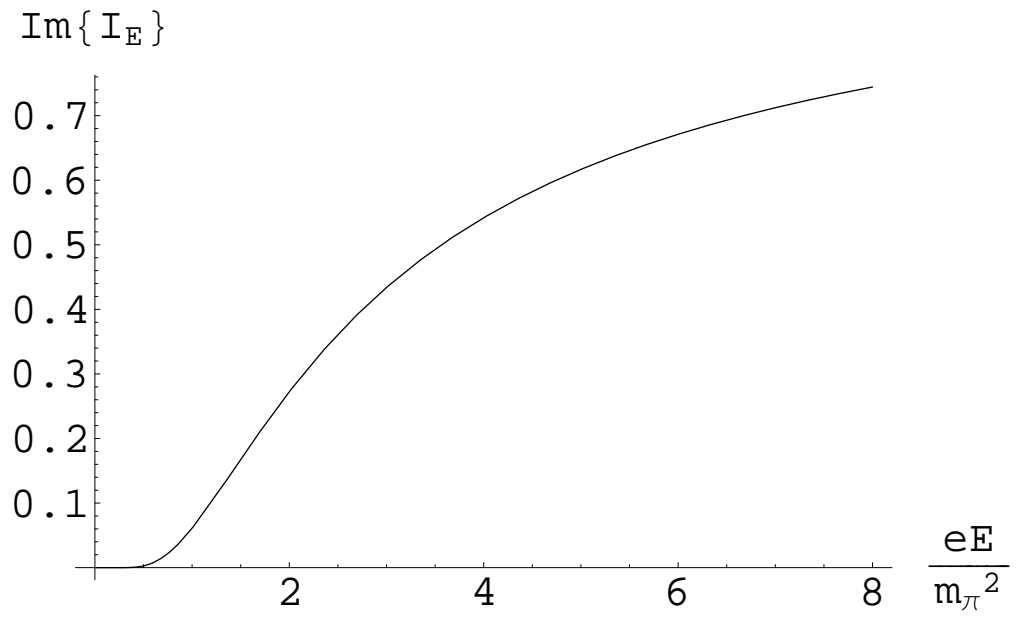
(b) $Im\{I_E\}$ vs eE/m_π^2

Figure 2.4: Real and imaginary parts of I_E defined in Eq. (2.35) are given in subfigures (a) and (b).
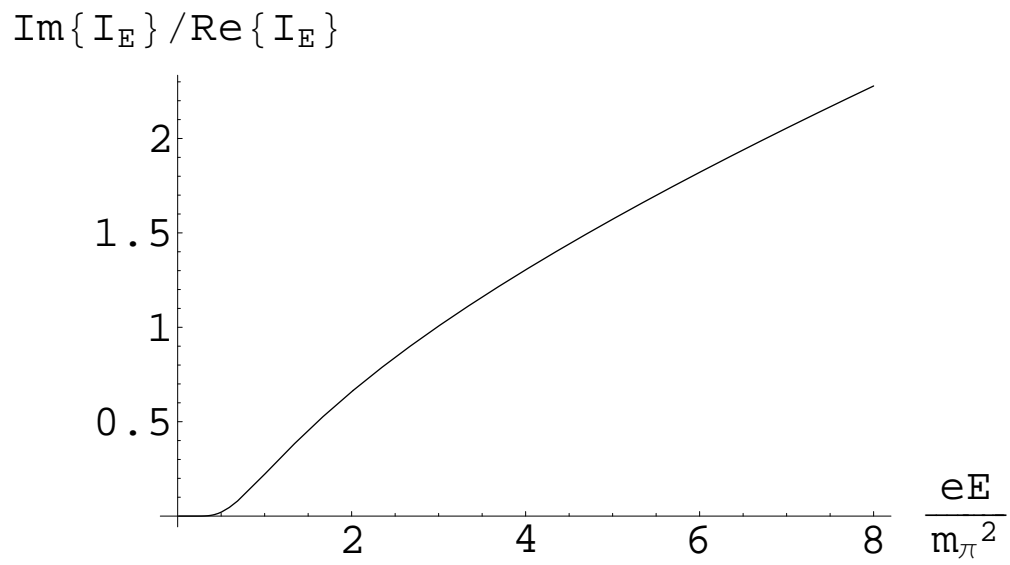
Figure 2.5: The ratio of the real and imaginary parts for the shift in the condensate

due to an electric field

The plots demonstrate explicitly, as expected, that the imaginary part of the answer can be neglected when $eE \ll m_\pi^2$ and abruptly becomes considerable, invalidating the shift in the condensate, as eE approaches m_π^2. Any shift beyond the field strength where the imaginary part becomes dominant will not be achievable in nature, because the vacuum will have disappeared before that shift can take place.

Thus, the shift in the chiral condensate in a constant electromagnetic field to one loop in χPT can be calculated as in Eq. (2.34), which is numerically identical to the analytically continued closed-form result given in Eq. (2.35). When $eE \ll m_\pi^2$, this shift is sensible and can be examined in the same way as the magnetic field. For larger electric fields, the answer is meaningless and the time-dependence of the Schwinger mechanism takes over.

2.5   General case: $\vec{E} \cdot \vec{H} \neq 0$

In the general case, unfortunately, unlike the case of a pure electric or a pure magnetic field, an elegant analytic solution is difficult to extract, so numerical calculations are the only way to analyze the shift in the condensate. Here, it is important to keep in mind that while the electric and magnetic fields are more intuitively comprehensible, the relevant variables are the Lorentz invariants. The system being in a "pure electric" field means that $\mathcal{F}$ is negative and $\mathcal{G} = 0$; a "pure magnetic" field means that $\mathcal{F}$ is positive and $\mathcal{G} = 0$. If both an electric and magnetic field are present, but they are orthogonal, one of these two results will apply, depending upon the sign of $\mathcal{F}$. The mixed general case that will be addressed in this section allows

$\mathcal{G} = E \cdot H \neq 0$, and both $\mathcal{F}$ and $\mathcal{G}$ can take on any value. Though the calculation here is analytically intractable, some of the methodology from the previous sections can aid in obtaining a numerical result.

The answer is ultimately given in terms of Lorentz invariants, but we have used "pure electric" and "pure magnetic" to refer to the fields in the frame which has been shifted so that the field is one or the other. Rather than using a specific frame, it will be illuminating in the general case to choose a new set of variables defined as in Ref. [100] by

$$\mathcal{F} = \frac{f^2 \cos(2\phi)}{2} \quad \mathcal{G} = \frac{f^2 \sin(2\phi)}{2} \tag{2.37}$$

with $\pi/2 \geq \phi \geq -\pi/2$. In fact, the domain can be restricted even further. The underlying theory, χPT, is parity-invariant, so any results must be parity-invariant; E and thus ϕ are parity-odd, so any result will ultimately be an even function of ϕ; for convenience, then, the domain can be limited at this early stage.

While the analysis will be with respect to these Lorentz invariants, it is useful to choose a particular frame to gain physical insight into the problem. In this case, in the frame where E is parallel to H, the newly defined variables are related to the physical fields as

$$H = f \cos(\phi) \quad E = f \sin(\phi) . \tag{2.38}$$

Thus, f is a measure of the overall strength of the field, whereas ϕ specifies how much the field resembles an electric field vs. a magnetic field. At $\phi = \pi/2$, the system is in the state of a pure electric field, and at $\phi = 0$, the system is in the state of a pure magnetic field.

Using the same expression for the effective lagrangian as specified in Eq. (2.30), but this time for the case where both $\mathcal{G}$ and $\mathcal{F}$ are nonzero and using the new variables f and ϕ, the shift in the condensate can again be obtained by differentiating with respect to m_π^2, yielding[100]

$$\Delta\Sigma(f,\phi) = \frac{ef\Sigma(0)\log 2}{16\pi^2 F_\pi^2} I_{EH}(f,\phi), \tag{2.39}$$

where $I_{EH}(f,\phi)$ is defined to be

$$I_{EH}(f,\phi) = \frac{1}{\log 2}\int_0^\infty \frac{du}{u^2} e^{-(m_\pi^2/ef)u}\left(\frac{u^2\sin(2\phi)}{2\sin\left(u\sin(\phi)\right)\sinh\left(u\cos(\phi)\right)+i\epsilon}-1\right), \tag{2.40}$$

As predicted, this integral cannot be evaluated analytically, and so further analysis will require numerical evaluation. The principal value and imaginary parts of the integral must first be extracted, as with the E field. This requires another imposition of a convention for the integration path, and the same condition is used as was used for the case of the E field and by Schwinger. The residues are, again, straightforward to extract, and the principal value can be separated using the same trick as for the E field in Eq. (2.36). The real and imaginary parts are then

$$\mathcal{R}(I_{EH}(f,\phi)) = I_{EH} - \frac{1}{\log 2}\sum_{n=1}^\infty \frac{\cos(\phi)(-1)^n e^{-n\pi m_\pi^2/(ef\sin(\phi))}}{\sinh(n\pi/\tan(\phi))} \tag{2.41}$$

$$\times \int_0^\infty \left(\frac{du}{u-\frac{n\pi}{\sin(\phi)}+i\epsilon}-\frac{du}{u+\frac{n\pi}{\sin(\phi)}+i\epsilon}\right) \tag{2.42}$$

$$\mathcal{I}(I_{EH}(f,\phi)) = \frac{1}{\log 2}\sum_{n=1}^\infty \frac{\pi\cos(\phi)(-1)^n e^{-n\pi m_\pi^2/(ef\sin(\phi))}}{\sinh(n\pi/\tan(\phi))}. \tag{2.43}$$

The principal value of the integral is plotted as a function of $\tan(\phi)$ and ef in fig. 2.6, and the imaginary part is plotted in fig. 2.7. Both figures are plotted as a function

of increasing ef/m_π^2 and also as a function of m_π^2/ef, to make asymptotic behavior at both extremes clear.

In the principal value plots, the curves for the mixed fields approach the curve for the E field at one extreme and the H field at the other extreme, as expected.

In the plots of the imaginary part, there is also a smooth transition from the case of the magnetic field, where there is no imaginary part and no pole creation, to the case of the electric field, with a maximal value for the imaginary part and the electric field. It is also clear that for large m_π^2, as expected, the imaginary part of the shift is suppressed regardless of the type of field. In this case, which is far from the $m_\pi = 0$ limit, it will be sensible to regard the principle value part of the shift as a physical shift in the chiral condensate, because not enough pairs will be created in a relevant time scale for the imaginary part to play a role. It is also the case that in the chiral limit, as discussed in previous work for the magnetic field[101], discussing the shift due to the electric field would not be sensible, because of this effect. Only when a finite m_π is present is it reasonable to discuss the effects of the electric field.

Another interesting characteristic of the plot of the poles is that in the limit of large m_π^2/ef, there is no difference between the shift due to the electric and magnetic fields, aside from a sign. This is the case generally for a mixed field where the electric and magnetic parts are interchanged. Mathematically, this means that $I_{EH}(f,\phi) \rightarrow -I_{EH}(f,\phi)$ when $\phi \rightarrow \pi/2 - \phi$. Therefore, in the absence of an imaginary part which will sap some of the effect of the electric field into the pair creation mechanism, the difference between the electric and magnetic fields is a change of sign. It is this regime which best highlights the difference between the
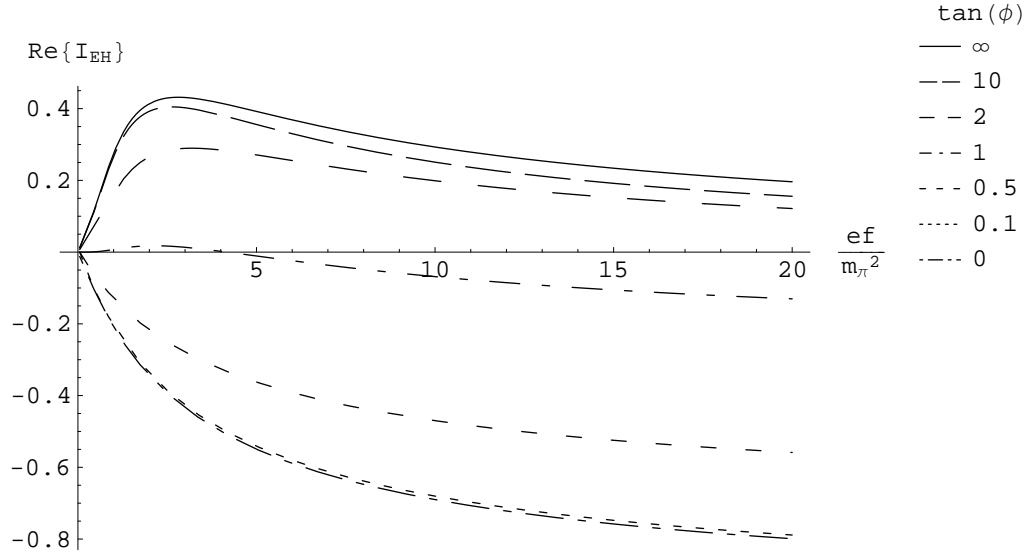
(a) $\mathcal{R}(I_{EH})$ vs ef/m_π^2
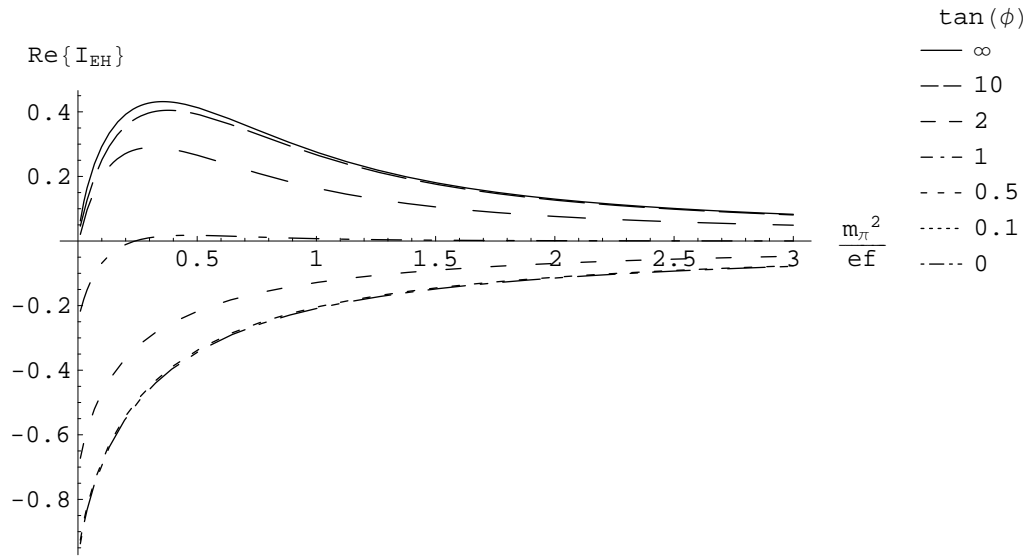
(b) $\mathcal{R}(I_{EH})$ vs m_π^2/ef

Figure 2.6: Principal value of the shift in the condensate plotted against the Lorentz invariants $\tan(\phi)$ and ef as defined in the text.
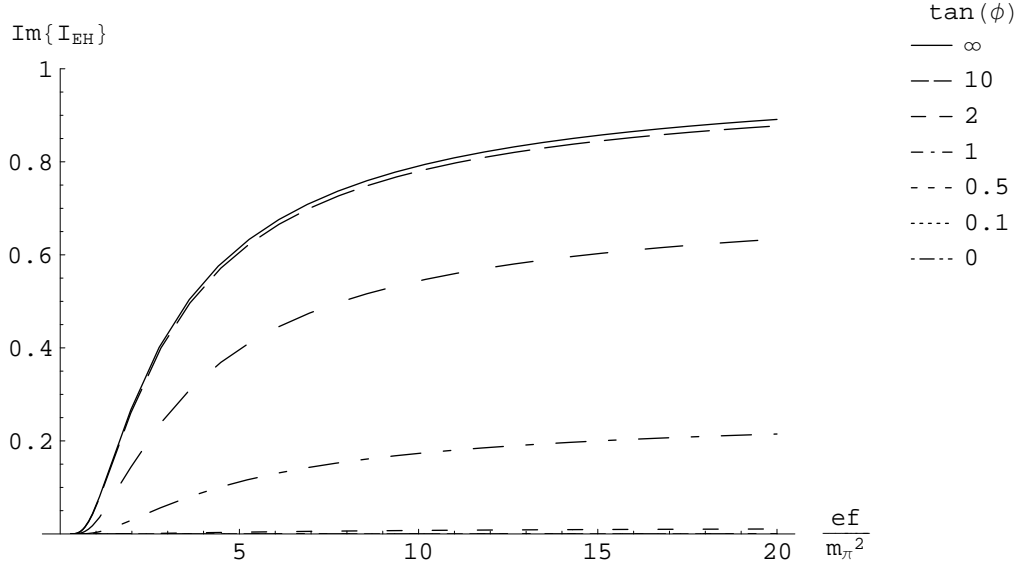
(a) $\mathcal{I}(I_{EH})$ vs ef/m_π^2

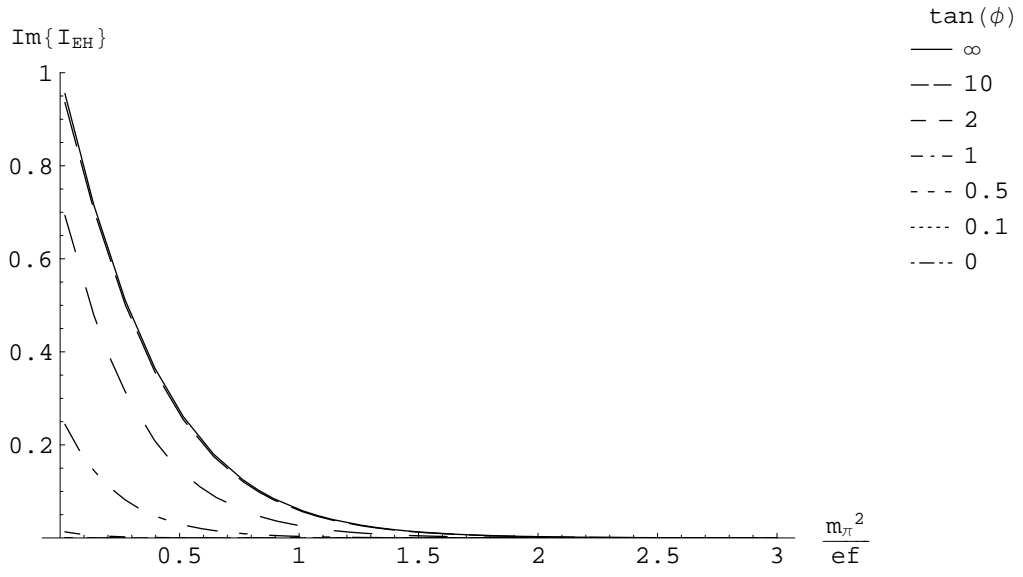(b) $\mathcal{I}(I_{EH})$ vs m_π^2/ef

Figure 2.7: Sum of the residues of the shift in the condensate plotted against the Lorentz invariants $\tan(\phi)$ and ef as defined in the text.

fields, that the magnetic field enhances the chiral condensate, while the electric field suppresses it.

In the opposite extreme, $m_\pi^2/ef = 0$, it is illuminating to consider the ratio of the real to imaginary parts of the result as a function of $\tan(\phi)$, as plotted in fig. 2.8. In the frame where E and H are parallel, this corresponds to E/H. The value of m_π^2/ef has been chosen to highlight the situation for each ϕ where the imaginary part is maximized. Predictably, the imaginary part becomes exponentially large as the field approaches a pure electric field, and is negligible when the electric field is less than half of the magnetic field, $\tan(\phi) \lesssim 0.5$. The instability due to the imaginary part can certainly not be neglected once the fields are of comparative magnitude, $\tan(\phi) \sim 1$.

Overall, then, the results of the general case are unsurprising once the electric and magnetic field results are known, showing a smooth mapping between them. The general numeric result is helpful, however, as in fig. 2.8, to determine how much electric field can be present before the pair creation mechanism becomes significant.

2.6 Discussion

Several methods for calculating the first-order shift in the chiral condensate due to a constant electromagnetic field, all derived from Schwinger's proper time formalism, have been discussed in this chapter. These include the NJL model, χPT in the chiral limit, and χPT for finite m_π. There are two expansion parameters which may be of relevance in these cases, eH and N_C.
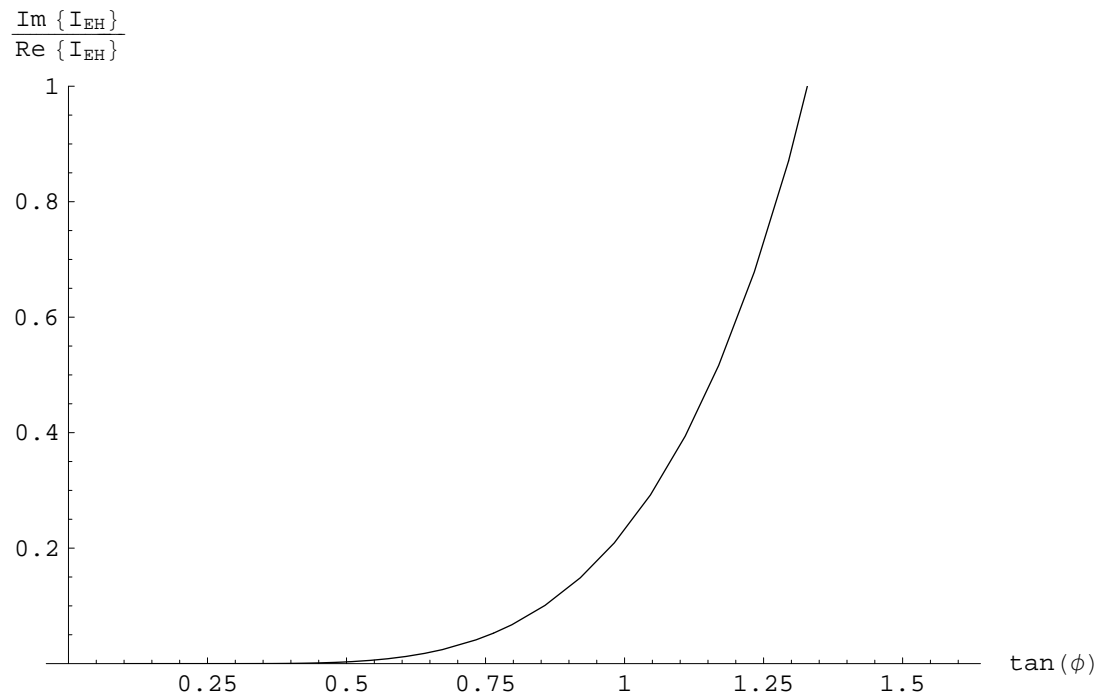
Figure 2.8: Ratio of the imaginary pair-creating piece versus the principal value, plotted as a function of $\tan(\phi)$ for $m_\pi^2/ef = 0$.

The NJL model was historically the first model to be used for this investigation. It has the advantage of being applicable up to higher energies than those which are possible in the chiral expansion, and includes quarks as a degree of freedom. However, it is limited by being only a model, lacking certain key features of QCD, such as confinement. Additionally, the regime where it can be assumed to be more useful, medium strength fields, is arguably less interesting than the lower energy regime; firstly, because such fields are less easily-achievable, and secondly, because an electromagnetic field in that regime is so large that the Schwinger pair creation mechanism will dominate, as discussed above. The leading-order shift for the magnetic field in this regime is shown to be proportional to $(eH)^2/\Sigma(0)^4$.

The chiral perturbation theory result at $m_\pi = 0$ is even more limited, requiring both a field large enough that m_π is negligible, but small enough that the perturbative expansion is still valid. As demonstrated by the finite m_π result, this regime is arguably not achievable, even in theory. The leading-order shift for the magnetic field in this case can be shown to be proportional to $(eH)/\Lambda^2 N_C$.

The result in χPT with finite m_π is far more flexible, but still has important limitations. It is clearly not valid in the limit where eH or $m_\pi^2 \sim \Lambda^2$, but has no limitations in terms of the relationship between eH and m_π, so has a well-defined region of validity, and can potentially address very small fields, which are more easily achievable in experiment. The experimental outlook is not as optimistic as this might imply, however, because the field must still be substantial in order for there to be a measurable effect on the chiral condensate; the issue has simply shifted from achievability to precision in measurement. Furthermore, the case for the electric

field continues to be problematic in this calculation, due to the creation of particle pairs from the vacuum. However, because this effect is less marked when the electric field is smaller, this regime is essentially the only one where a physical shift in the condensate due to the electric field is calculable. The calculation demonstrates that for a magnetic field, a small electric field, or a large mixed field where the magnetic field portion is at least $\sim 2\times$ as strong as the electric field, it is sensible to discuss the shift in the condensate. In this case, the shift due to the magnetic field is $f(m_\pi^2/eH)eH/\Lambda^2 N_C$.

The results from the NJL model and the χPT expansion are not in agreement, which is due to the non-commutativity of the small eH and large-N_C limits, as can be seen from the leading order terms in the expansion. It is desirable to understand when these results can be brought into agreement, and this can be achieved by performing a higher-order calculation. Because of the limitations of the NJL model, as well as the difficulties in obtaining a higher-order result, it is clearly beneficial to perform the calculation in χPT. The prior work of Ref. [109] discusses the higher-order result in the chiral limit, and Ref. [110] discusses the higher-order result with finite m_π. These results will be considered in the following chapter.

Chapter 3

External Electromagnetic Field at Next-To-Leading Order in χPT

This chapter discusses how the results of the previous chapter can be expanded to analyze the effects of an electromagnetic field in chiral perturbation theory to $\mathcal{O}(p^6)$. In doing so, it follows closely the results of Ref. [110].

As discussed in the previous chapter, it is interesting to examine the effects of an electromagnetic field of a strength corresponding to low energies, with $eH \ll \Lambda_H^2$. The ideal tool to study such effects is chiral perturbation theory, which is applicable within this energy range. In the prior chapter, the effects of this field at lowest order in chiral perturbation theory were examined. However, there are some inconsistencies in the answers obtained via chiral perturbation theory and the NJL model. Of course, it is possible to dismiss the NJL results as "just a model," but the result in the NJL model has qualitatively different dependencies from the χPT result in the relevant expansion terms, eH and N_C. Presumably, if it has any validity at all, the NJL result ought to correspond to the χPT result in some limit. There are no terms in χPT to order $\mathcal{O}(p^4)$ which match, but there are potential terms at $\mathcal{O}(p^6)$ which appear to have a similar structure. Regardless, χPT at $\mathcal{O}(p^6)$ is more accurate than the lower order result, particularly on the border of the regime of validity.

As was the case for the $\mathcal{O}(p^4)$ case, prior work at $\mathcal{O}(p^6)$ focused on the chiral

limit[109]. The same limitations for the chiral limit apply at $\mathcal{O}(p^6)$ as applied at $\mathcal{O}(p^4)$, but are more acute. Not only will the free propogator be evaluated differently (the same as at $\mathcal{O}(p^4)$, but there will be additional terms for finite m_π which were not included at $m_\pi = 0$.

Increased precision of a result from higher orders of calculation is always of interest. As mentioned, however, the disagreement in lower orders of calculation makes the higher order result more compelling. One important aspect of this disagreement comes from large-N_C QCD[24, 22, 23]. The chiral expansion is in terms of momentum order, but the N_C dependence of the LECs varies from LEC to LEC. The $\mathcal{L}_2$ LECs which correspond to usual physical parameters, M_π and F_π, have the same N_C dependence as they always do ($M_\pi \propto N_c^0$, $F_\pi \propto N_c^{1/2}$). However, in order to make the χPT processes consistent with QCD, LECs in the higher-order lagrangians can and must have nontrivial N_C dependence. The rule for determining this dependence is straightforward: The N_C dependence of a particular LEC is controlled by the number of flavor traces in the term it multiplies. A flavor trace occurs when there is a quark loop in the corresponding QCD calculation. Large-N_C counting rules for QCD, as discussed in the previous chapter, indicate that each quark loop reduces the order of a diagram by an order of N_C (this is generally qualified to include only internal quark loops, but only because diagrams with different external lines represent different processes). In order to equate the χPT process to the QCD process, some extra N_C dependence must be introduced, and the only parameters available to absorb this dependence are the LECs. Thus, each LEC is down by one power of N_C for every flavor trace in its multiplying term.

This large-N_C dependence may be related to the chiral expansion. This convergence has been tested using a number of known processes which can be calculated to two-loop order[39]. The difference between the $\mathcal{O}(p^4)$ result and the $\mathcal{O}(p^6)$ is often very small, with very little quantitative and no qualitative difference. In some cases, however, such as the calculation of the process $\gamma\gamma \to \pi^0\pi^0$, the $\mathcal{O}(p^6)$ result is persuasively more accurate than the $\mathcal{O}(p^4)$ result[111]. This sort of correction is desirable in the sense that it indicates that the chiral expansion produces an accurate result, but that it comes at next-to-leading order means that the expansion parameter is not very small and that higher order terms can be important. The case of the shift of the chiral condensate due to an electromagnetic field was obviously not part of the analysis in Ref. [111], but the relevant LEC is derived from the same $\gamma\gamma \to \pi^0\pi^0$ process which produced a large qualitative difference at $\mathcal{O}(p^6)$, so it is conceivable that the next-to-leading order result will be important here, as well.

This chapter discusses the necessary parts of χPT in more depth than in Chapt. 1, then proceeds with the calculation of the correction to the vacuum energy at $\mathcal{O}(p^6)$, including its renormalization.

3.1   Chiral Perturbation Theory

An introduction to the basics of χPT was provided in Section 1.2.2. The calculation of Chapt. 2 was technically in χPT, but only uses the lowest-order lagrangian, which includes electromagnetic fields only in the minimally coupled way, and thus only needs the Schwinger propogator to determine the shift. At $\mathcal{O}(p^6)$, the shift will

include not only terms added from the $\mathcal{O}(p^4)$ lagrangian, but terms from the $\mathcal{O}(p^6)$ lagrangian, as well.

It is important to understand how various diagrams contribute to the calculation at each order. In general, each loop contributes an order of p^2, in addition to the powers of momentum from the vertices in the diagram. Diagrams contributing to the vacuum shift in the condensate at any order do not have external legs other than those from the constant electromagnetic field. The lowest order term would be a tree-level diagram using the $\mathcal{L}_2$ lagrangian, but no such diagrams contribute as there can be no vertices which contain both m_π and the electromagnetic field in $\mathcal{L}_2$. The next order of calculation is $\mathcal{O}(p^4)$, as calculated in Chapt. 2. The possibilities for terms which might contribute at this order would be one-loop terms with the $\mathcal{L}_2$ lagrangian and tree-level terms at $\mathcal{O}(p^4)$. However, the latter do not exist, as tree level terms require both the electromagnetic field and m_π; to remain Lorentz invariant, the electromagnetic field must appear either twice or contracted with a pion field. The latter is obviously excluded for a tree diagram, and the former would be too high-order to also include orders of m_π, so it is also excluded. At $\mathcal{O}(p^6)$, terms contributing are two-loop order in $\mathcal{L}_2$, one-loop order in $\mathcal{L}_4$, and tree-level in $\mathcal{L}_6$. Here, all three sorts of terms do exist. For the first time, it is possible to have tree-level terms multiplying $m_\pi^2(eF)^2$, which is the lowest-order possibility for a tree-level calculation of the shift.

With this discussion of the terms which will be possible, the term which is

relevant to this calculation can be picked out of the $\mathcal{L}_6$ lagrangian. It is[37]

$$\mathcal{L}_6 = c_{34}\langle\chi_+ f_{+\mu\nu} f_+^{\mu\nu}\rangle + \sum_{i\neq 34} c_i P_i, \tag{3.1}$$

where the $c_i P_i$ are the other terms in the expansion which do not contribute to the calculation at hand.

For this calculation, as with all calculations, some renormalization will be required. Chapt. 1 discussed how χPT can be renormalized order-by-order. Gasser and Leutwyler calculated the explicit form for the counterterms required[18, 19], with the result that the $\mathcal{L}_4$ LECs can be expressed as

$$l_i = (c\mu)^{d-4} (l_i^r + \gamma_i \Lambda)$$

$$\Lambda = \frac{1}{16\pi^2(d-4)}$$

$$\gamma_1 = \frac{1}{3}, \gamma_2 = \frac{2}{3}, \gamma_3 = -\frac{1}{2}, \gamma_4 = 2, \tag{3.2}$$

$$\gamma_5 = -\frac{1}{6}, \gamma_6 = -\frac{1}{3}, \gamma_7 = 0$$

When $M \neq 0$, these can be expressed in terms of scale-independent parameters $\bar{l}_i$ as

$$l_i^r = \frac{\gamma_i}{32\pi^2} \left(\bar{l}_i + \log\frac{M^2}{\mu^2}\right). \tag{3.3}$$

The $\mathcal{L}_6$ term can be renormalized as calculated in Ref. [38] using the expression

$$c_i = \frac{(c\mu)^{2(d-4)}}{F^2} \left(c_i^r(\mu, d) - \gamma_i^{(2)}\Lambda^2 - (\gamma_i^{(1)} + \gamma_i^{(L)}(\mu, d))\Lambda\right)$$

$$\gamma_{34}^{(L)} = -l_5^r + \frac{1}{2}l_6^r, \gamma_{34}^{(1)} = \gamma_{34}^{(2)} = 0, \tag{3.4}$$

which will allow a finite result using the renormalized LECs to be calculated.

3.2 Calculation of Σ from vacuum energy

The shift in the chiral condensate due to the electromagnetic field, $\Delta\Sigma$, can be calculated at this order from the vacuum energy in the same way as described in Chapt. 2, using the equation

$$\Sigma = -\frac{\partial \epsilon_{\text{vac}}}{\partial \hat{m}}. \tag{3.5}$$

However, the GMOR relation, $F_\pi^2 M_\pi^2 = \Sigma(m_u + m_d)$, is only accurate to first order, and so some ambiguity is introduced. The chiral condensate and the quark mass are not independent, with only their product being an experimentally measurable number. This product can be derived to be

$$2\hat{m}\Sigma = F^2 M^2 \left\{ 1 + \frac{M_\pi^2}{32\pi^2 F_\pi^2}(4\bar{h}_1 - \bar{l}_3) + \mathcal{O}(M_\pi^4) \right\}. \tag{3.6}$$

The LEC $\bar{h}$ is unphysical, and will vary with normalization condition. The ambiguity is in the definition of Σ, so in order to avoid it, it is possible to define the quantity Σ_0 using the equation,

$$2\hat{m}\Sigma_0 = F_\pi^2 M_\pi^2, \tag{3.7}$$

which allows all results to be expressed as a function of $\Delta\Sigma/\Sigma_0$, where $\Delta\Sigma$ is only expressed as a function of H, or $\Delta\Sigma \equiv \Sigma(H) - \Sigma(H = 0)$. The result will then be well defined at order $\mathcal{O}(p^6)$.

Another important difference at $\mathcal{O}(p^6)$ is that at this order, F_π and M_π are not identical to the $\mathcal{L}_2$ LECs. When all terms in a calculation are of the same order, this is irrelevant, because any such corrections will be beyond the scope of the calculation. However, at $\mathcal{O}(p^6)$, the corrections to the $\mathcal{L}_2$ LECs appearing at

$\mathcal{O}(p^4)$ will be of the same order as the $\mathcal{O}(p^6)$ terms. One correction term will be sufficient to increase the level of accuracy in this case. Expressing M_π and F_π as functions of the LECs $M \equiv 2B\hat{m}$ and F produces[18]

$$M_\pi^2 = M^2 \left[1 - \frac{M^2}{32\pi^2 F^2} \bar{l}_3 + \mathcal{O}(M^4) \right]$$
$$F_\pi = F \left[1 + \frac{M^2}{16\pi^2 F^2} \bar{l}_4 + \mathcal{O}(M^4) \right]. \tag{3.8}$$

Again, these corrections need only be applied to the $\mathcal{O}(p^4)$ calculations, because at $\mathcal{O}(p^6)$ they will be beyond the stated accuracy of the calculation.

With the $\mathcal{O}(p^4)$ terms modified with the LECs to higher accuracy for $\mathcal{O}(p^6)$, it is then necessary to enumerate the new diagrams which contribute to the vacuum energy at this order. As discussed in the introduction, these new terms will include two-loop order terms from the $\mathcal{L}_2$ lagrangian, one-loop terms from the $\mathcal{L}_4$ lagrangian, and even a tree level term from the $\mathcal{L}_6$ lagrangian. There are two further require-ments for diagrams that can contribute–first, obviously, they must be dependent on the electromagnetic field, otherwise they will cancel in the electromagnetic field. Second, they must contain at least one power of M_π, so that there is a nonzero result when the derivative with respect to this quantity is taken. With these criteria, the diagrams which contribute at $\mathcal{O}(p^6)$ are those depicted in Fig. 3.1.

The form of these terms is dictated by the symmetries of QCD. In the $\mathcal{L}_4$ lagrangian, the contributing terms are those proportional to l_3, l_5 and l_6. In $\mathcal{L}_6$, the only term contributing is c_{34}. Using the Weinberg parameterization of Eq. (1.9) in $SU(2)$, as discussed previously, and taking $m_u = m_d$, the contributing terms from

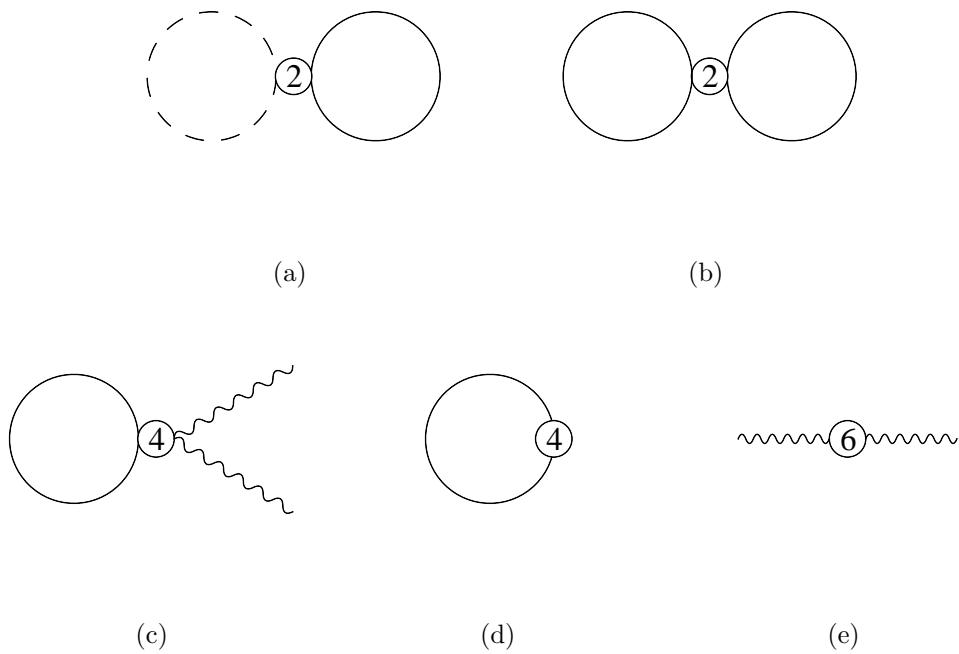(a)   (b)

(c)   (d)   (e)

Figure 3.1: Diagrams contributing to the vacuum energy shift due to an electro-magnetic field. Dashed lines denote π^0 and solid lines denote $\pi^{\pm}$.

all three levels of the lagrangian can be written explicitly as[109, 110]

$$\mathcal{L}_2 = \frac{1}{2}(\partial_\mu \pi^0)^2 - \frac{M^2(\pi^0)^2}{2} - M^2 \pi^+ \pi^-$$

$$+ (\partial_\mu \pi^+ + ieA_\mu \pi^+)(\partial^\mu \pi^- - ieA^\mu \pi^-)$$

$$+ \frac{1}{2F^2} \left[\pi^0 \partial_\mu \pi^0 + \partial_\mu (\pi^+ \pi^-) \right]^2$$

$$- \frac{M\pi^2}{8F^2} \left[2\pi^+ \pi^- + (\pi^0)^2 \right]^2$$

$$\mathcal{L}_4 = -\frac{2l_5}{F^2}(eF_{\mu\nu})^2 \pi^+ \pi^-$$

$$- \frac{2il_6}{F^2} eF_{\mu\nu} \left[\partial^\mu \pi^- \partial^\nu \pi^+ + ieA^\mu \partial^\nu (\pi^+ \pi^-) \right]$$

$$- 2l_3 \frac{M^4}{F^2} \pi^+ \pi^-$$

$$\mathcal{L}_6 = 4c_{34} M^2 (eF_{\mu\nu})^2.$$

(3.9)

The simplest case, as at the $\mathcal{O}(p^4)$ level, is that of a pure magnetic field, which is simpler than a pure electric field because it does not contain any imaginary part. This will be extended later to the case of a pure electric fields, which will have analytic results similar to those of the pure magnetic field case, and to the mixed E and H field case, which is only tractable numerically.

In the expansion to $\mathcal{O}(p^6)$, it will be necessary to use not just the vacuum energy as calculated by Schwinger[75], but the explicit propagator for a scalar particle in an H field, which was also first derived by Schwinger, but was recast in a more useable form in Ref. [109] as

$$D^H(x, y) = \Phi(x, y) \int \frac{d^4 k}{(2\pi)^4} e^{ik(x-y)} D^H(k)$$

$$D^H(k) = \int_0^\infty \frac{ds}{\cosh(eHs)} e^{-s\left(k_\parallel^2 + k_\perp^2 \frac{\tanh eHs}{eHs} + M^2\right)},$$

(3.10)

where $\Phi(x, y) = \exp\{ie \int_y^x A_\mu(z)dz_\mu\}$, $k_\parallel^2 = k_3^2 + k_4^2$ and $k_\perp^2 = k_1^2 + k_2^2$.

For a propagator closed in on itself, this will be normalized by the scalar propagator without an electromagnetic field, whose explicit form will also be of use, and can be written

$$D(0) \equiv D(x, x) = \int \frac{d^d k}{k^2 + M^2}$$

$$= 2M^2 (c\mu)^{d-4} \left[\Lambda + \frac{1}{32\pi^2} \log \frac{M^2}{\mu^2} \right] \tag{3.11}$$

$$\Lambda = \frac{1}{16\pi^2 (d-4)}.$$

Thus, although $D(0)$ and $D^H(0) \equiv D^H(x, x)$ are both divergent, the $H = 0$ propagator can be subtracted to obtain a finite result, with

$$D^{\Delta H}(0) \equiv D^H(0) - D(0)$$

$$= - \frac{eH}{16\pi^2} \int_0^\infty \frac{dx}{x^2} e^{-\beta x} \left(1 - \frac{x}{\sinh x} \right), \tag{3.12}$$

where the parameter $\beta \equiv M^2/eH$. The integral is of the same form as the one calculated in Ref. [100] and discussed in Chapt. 2, and is simplifies the propagator to the expression

$$D^{\Delta H}(0) = - \frac{eH}{16\pi^2} I_H(\beta)$$

$$I_H(\beta) = \log(2\pi) + \beta \log \left(\frac{\beta}{2} \right) - \beta - 2 \log \Gamma \left(\frac{1+\beta}{2} \right). \tag{3.13}$$

The simplified forms of the relevant terms can be used to calculate the vacuum energy contributions from each of the diagrams, resulting in[109, 110]

$$\epsilon_{3.1(a)}^{(2)} = \frac{M^2}{2F^2} D(0) D^H(0)$$

$$\epsilon_{3.1(b)}^{(2)} = \frac{1}{F^2} D^H(0) \int \frac{d^d k}{(2\pi)^d} (k^2 + M^2) D^H(k)$$

$$\epsilon_{3.1(c)}^{(2)} = \frac{2(eH)^2}{F^2} (2l_5 - l_6) D^H(0) \tag{3.14}$$

$$\epsilon_{3.1(d)}^{(2)} = 2l_3 \frac{M^4}{F^2} D^H(0)$$

$$\epsilon_{3.1(e)}^{(2)} = - 8c_{34} M^2 (eH)^2.$$

The notation $\epsilon^{(2)}_{3.1(x)}$ refers to the vacuum energy contribution resulting from the diagram in subfigure (x) of fig. 3.1. The total vacuum energy contribution at second order will later be denoted as $\epsilon^{(2)}$.

The calculation of $\epsilon^{(2)}_{3.1(b)}$ is the only one which has a more complicated integral than that for $D^H(0) - D(0)$, but upon explicit calculation, this diagram vanishes generally, not just in the $M_\pi = 0$ case considered by Ref. [109].

While the divergences with no dependence at all on the electromagnetic field can always be immediately neglected, there is some delicacy in parts of the renormalization, as counterterms will be required. However, these counterterms have been calculated generally for the LECs in both $\mathcal{L}_4$[18] and $\mathcal{L}_6$[38]. To be reassured more explicitly that all these cancellations take place as they should, it is convenient to express $D^H(0)$ as a combination of a finite and an infinite piece, $D^H(0) = D^{\Delta H}(0) + D(0)$. Divergences due only to $D(0)$ which do not multiply H are immediately ignored, and those which do multiply H must be carefully examined for renormalization. Specifically, the $\mathcal{L}_2$ term $\epsilon^{(2)}_{3.1(a)}$ is a divergent term, which is cancelled by the renormalization of the $\mathcal{L}_4$ term l_3. Similarly, the $\mathcal{L}_4$ term $\epsilon^{(2)}_{3.1(c)}$ has a finite piece which contributes to the calculation, and a divergent piece which is cancelled by the renormalization of the $\mathcal{L}_6$ LEC c_{34}. The final two contributions, $\epsilon^{(2)}_{3.1(d)}$ and $\epsilon^{(2)}_{3.1(e)}$, do not have any explicit divergences, aside from the counterterms which they must include to cancel the divergences of the other terms.

Combining all these terms into the full contribution to the vacuum energy at

$\mathcal{O}(p^6)$ results in

$$\epsilon^{(2)}(H) = -\frac{(eH)^3}{(16\pi^2)^2 F^2}\left\{ I_H(\beta)\left[\frac{1}{3}(\bar{l}_6 - \bar{l}_5) - \frac{\beta^2}{2}\bar{l}_3\right] + \beta\bar{d}(M^2)\right\}. \tag{3.15}$$

The $\bar{l}_i$ have standard definitions as the scale-independent values for the LECs. The scale-independent quantity $\bar{d}$ has been defined here and can be written explicitly as

$$\bar{d}(M^2) = 8(16\pi^2)^2 c_{34}^r - \frac{1}{3}(\bar{l}_6 - \bar{l}_5)log\left(\frac{M^2}{\mu^2}\right). \tag{3.16}$$

Eq. (3.15) is an explicit form for the vacuum energy using new diagrams for $\mathcal{O}(p^6)$. These must be combined with the result of substituting the next-order calculation of M_π in the $\mathcal{O}(p^4)$ result from Chapt. 2. This substitution cancels the $\bar{l}_3$ term (the correction to F only appears at second order, and therefore is not relevant in this calculation). Finally, taking the derivative of the combined vacuum energy and applying the GMOR relation, the shift in the condensate can be expressed

$$\frac{\Delta\Sigma(H)}{\Sigma_0} = \frac{eH}{16\pi^2 F_\pi^2}I_H(\beta_\pi) + \left(\frac{eH}{16\pi^2 F_\pi^2}\right)^2$$
$$\times \left\{ -\frac{1}{3}(\bar{l}_6 - \bar{l}_5)\left[1 + \log 2 + \psi\left(\frac{1+\beta_\pi}{2}\right)\right] + \bar{d}(eH)\right\}, \tag{3.17}$$

with $\psi(x) \equiv \frac{d}{dx}\log\Gamma(x)$ and $\beta_\pi \equiv M_\pi^2/eH$.

This shift should agree with the result in the chiral limit when $\beta \to 0$, and indeed, in this case $\psi\left(\frac{1}{2}\right) = -\gamma_e$ and the shift is identical to that derived in Ref. [109].

The translation to the E field is again straightforward, with the substitution $H \to iE$ yielding a similar analytic expression. The generalization to the $E \cdot H \neq 0$ case is, of course, far more complicated, and unfortunately yields an expression which is not analytically tractable–unsurprising, as the $\mathcal{O}(p^4)$ result was also not analytically tractable. As in Chapt. 2, the result will most conveniently be expressed

in terms of the variables f and ϕ, defined by $\mathcal{F} = \frac{f^2 \cos(2\phi)}{2}$ and $\mathcal{G} = \frac{f^2 \sin(2\phi)}{2}$. Because the result of the above calculation depends only on the H field through the propagator as calculated by Schwinger, the calculation of the integral is the same as in the $\mathcal{O}(p^4)$ case, and the generalized form of the integral can be written

$$
\begin{aligned}
\frac{\Delta\Sigma(\mathcal{F},\mathcal{G})}{\Sigma_0} =& \frac{ef}{16\pi^2 F_\pi^2} I_{EH}(\beta_f, \phi) + \left(\frac{ef}{16\pi^2 F_\pi^2} \right)^2 \cos 2\phi \\
& \times \left\{ \frac{1}{3}(\bar{l}_6 - \bar{l}_5)(I'_{EH}(\beta_f, \phi) - 1) + \bar{d}(M_\pi^2) \right\}
\end{aligned}
\tag{3.18}
$$

$$
I_{EH}(\beta_f, \phi) = \int_0^\infty \frac{dz}{z^2} e^{-\beta_f z} \left[1 - \frac{z^2 \sin 2\phi}{2 \sin(z \sin \phi) \sinh(z \cos \phi) + i\epsilon} \right].
$$

As the integral is the same as that discussed in Ref. [100] and Chapt. 2, it will again have some potential ambiguity. The integral has divergences from its poles, which are interpreted using the Schwinger mechanism as pair creation in an electric field to whatever degree it is present. The divergence is regulated in the same manner as in the prior result, which is a physical choice corresponding to pair creation. As in the prior result, the magnitude of the imaginary part of the result is taken as a rough indicator of the importance of the instability.

3.3 Numerical results

The structure of χPT is due only to the symmetries of QCD, so it is plausible to say that the content of the theory is encoded only in the values of the LECs, which must be measured from known processes. The $\mathcal{L}_2$ LECs were, of course, very well known experimentally from an early stage, and the uncertainties on the $\mathcal{L}_4$ LECs, while not as small, are still very manageable and lead to relatively insensitive results. The situation with the $\mathcal{L}_6$ LECs is unfortunately far less satisfactory. This is natural,

as the number of processes that can be used to measure the $\mathcal{L}_6$ LECs is generally far less than the number of LECs themselves. In addition to the uncertainty in its magnitude, the LEC necessary in this calculation, c_{34}, has an additional difficulty as it only contributes to resonance processes involving scalar exchange where it appears squared, and thus its sign remaines undetermined. The complete ambiguity in sign occurs at the scale of these resonance processes, $\sim M_\rho = 768\text{MeV}[111]$, so it is the scale-dependent experimental value which has an undetermined sign. The quantity $\bar{d}$ used in this discussion is positive in both cases, but the ambiguity in the sign of the scale-dependent LEC makes its uncertainty very large.

With these discussions in mind, the relevant experimental values for the processes discussed here are[111, 112]

$$\bar{l}_6 - \bar{l}_5 = 3.0 \pm 0.3$$

$$d^r(768\text{Me}V) \equiv 8(16\pi^2)^2 c_{34}^r = \pm 1.5 \pm 1.5,$$

(3.19)

where the value of the constant d^r at the measured scale has been listed. The uncertainty of this estimate is obviously too great to make a real quantitative determination of the $\mathcal{O}(p^6)$, but some information may still be forthcoming.

With these values, the shift in the condensate can be plotted up to the level of precision which is available. The first piece of data is to compare the value of the shift in a pure magnetic field for a finite M_π to the value of the shift when $M_\pi = 0$, to see how much the result is improved by a more realistic calculation. This comparison is plotted in fig. 3.2. This plot, which includes both the $\mathcal{O}(p^4)$ shift and the $\mathcal{O}(p^6)$ shift, shows a significant difference when a finite M_π is included, and that even with the large uncertainty in d^r, there is no possibility of overlap.
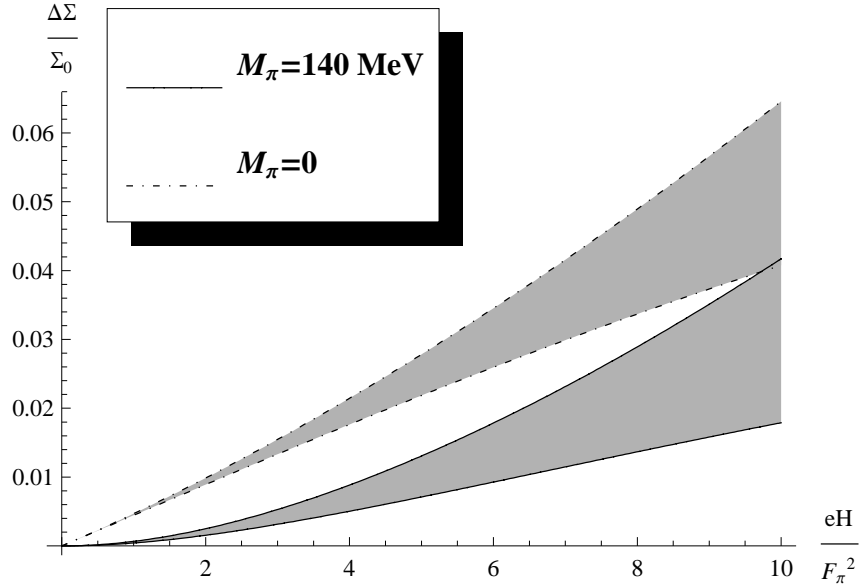
87

Figure 3.2: A comparison of the shift due to a pure magnetic field in the $M_\pi = 0$ case to the $M_\pi = 140$ MeV case. Shaded regions indicate uncertainty due to the $\mathcal{L}_6$ constant d^r.

The difference in the $\mathcal{O}(p^6)$ contribution alone is also of interest, and is plotted in fig. 3.3. The contribution of this portion alone is fairly close in the $M_\pi = 0$ vs. the finite M_π case, however, because the shift at this order is less in the finite case, the $\mathcal{O}(p^6)$ portion is potentially more significant as a percentage of the total shift.

Another interesting limit is the one opposite to that calculated previously, namely $M_\pi^2 \gg eH$ (or $\beta_\pi \to \infty$). The analytical expression in this case is

$$\frac{\Delta\Sigma(H)}{\Sigma_0} = \frac{eH}{16\pi^2 F_\pi^2}\left(\frac{F_\pi^2}{6M_\pi^2} - \frac{\bar{l}_6 - \bar{l}_5}{48\pi^2} + \frac{\bar{d}}{16\pi^2}\right), \qquad (3.20)$$

which disappears as $\beta_\pi \to \infty$ (no magnetic field). This encodes the low-energy behavior in a perfectly sensible experimental regime, namely that of a finite pion mass and a very small external field. This regime is the one most likely in experi-
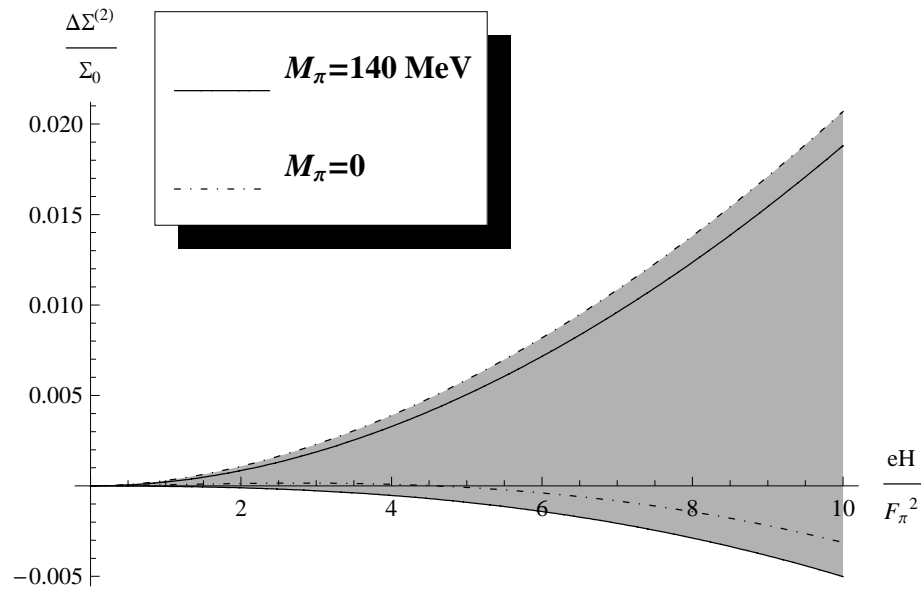
Figure 3.3: A comparison of the shift due to a pure magnetic field in the $M_\pi = 0$ case to the $M_\pi = 140$ MeV case, using only the $\mathcal{O}(p^6)$ portion. Shaded regions indicate uncertainty due to the $\mathcal{L}_6$ constant d^r.

ment, which as discussed previously, can only achieve very small values for the ratio eH/M_π^2.

For the case of generalized E and H fields, the numerical trick used in Ref. [100] and Chapt. 2 is still applicable to separate the principal value part of the integral from the imaginary part due to the poles. Subtracting the expression

$$i \sum_n R_n(z_n) \left(\frac{1}{z - z_n} - \frac{1}{z + z_n} \right). \tag{3.21}$$

from the integral will yield the principal value. This expression has all the poles of the original integral, but when integrated, its principal value is obviously zero by symmetry.

This method allows the total shift in the condensate due to a generalized electromagnetic field to be plotted up to $\mathcal{O}(p^6)$. The real and imaginary parts of the shift are plotted in fig. 3.4, and the ratio of the added correction from $\mathcal{O}(p^6)$ to the total shift in the condensate is plotted in fig. 3.5. In these plots, as well as the prior ones, the shaded region indicates the possible values for the shift, based on a d^r which can vary within the range $(-3, 3)$. In these figures, the value of $ef/F_\pi^2 = 10$ corresponds to a value of $ef = 290$ MeV (the expansion parameter is $\Lambda_H = 4\pi F_\pi = 1.2$ GeV).

From Fig. 3.5 and Eq. (3.20), it is clear that the $\mathcal{O}(p^6)$ correction is potentially significant for some d^r values within the experimentally estimated range, but that other d^r values result in very little impact. In particular, positive d^r would result in a significant difference between the $\mathcal{O}(p^6)$ calculation and the $\mathcal{O}(p^4)$ calculation, whereas a negative value for the shift is negligible until large values for ef/F_π^2 are
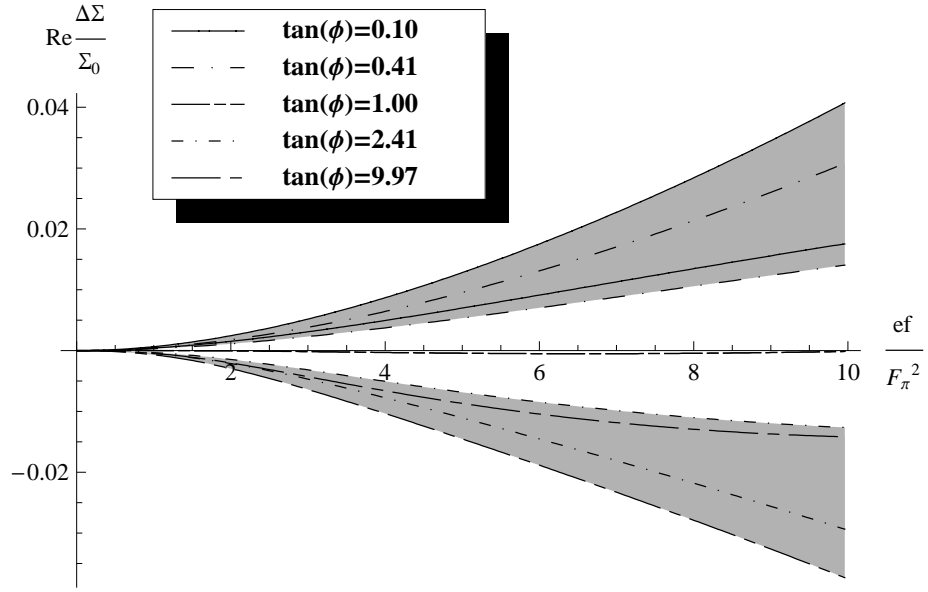
(a)
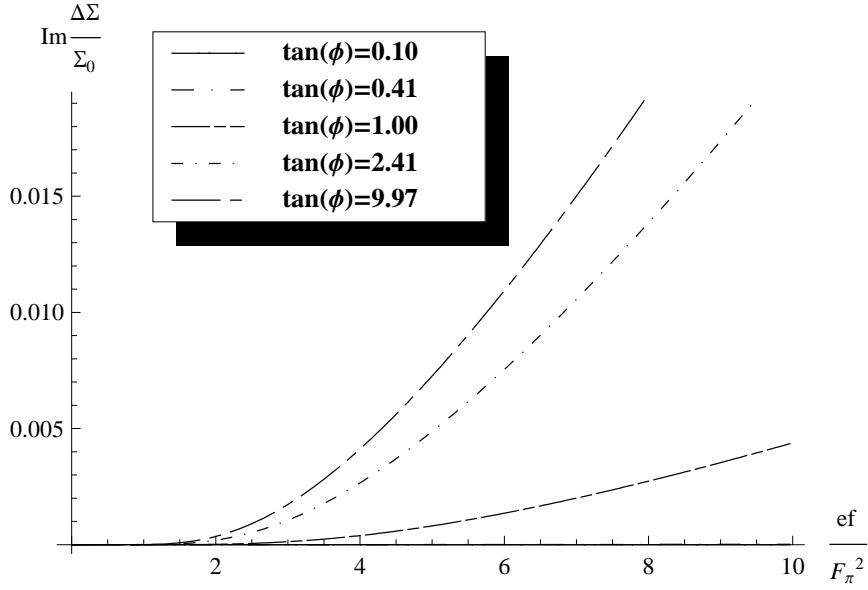
(b)

Figure 3.4: The imaginary and real parts of the total value of the shift in the condensate due to general E and H fields, with f and ϕ as defined in the text. Shading depicts uncertainty due to c_{34}.

.
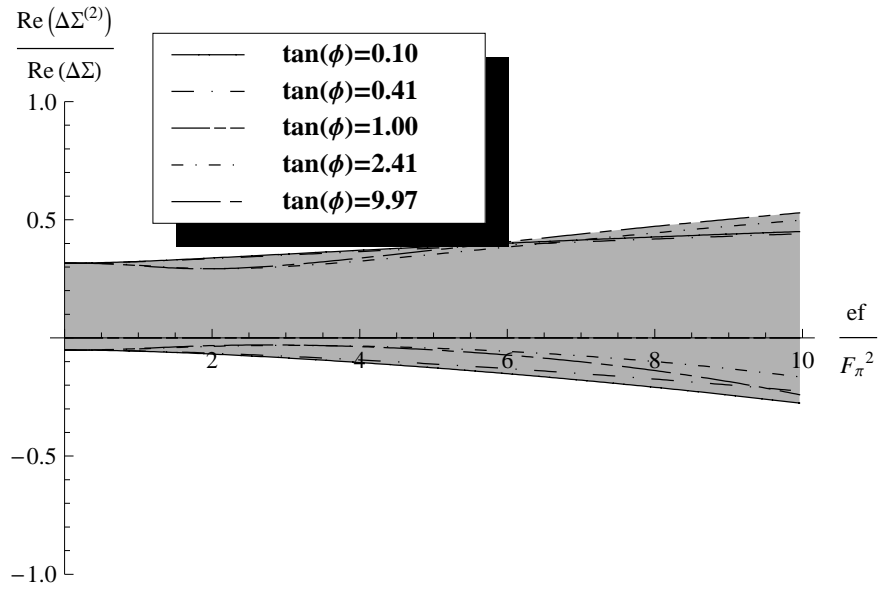
(a)
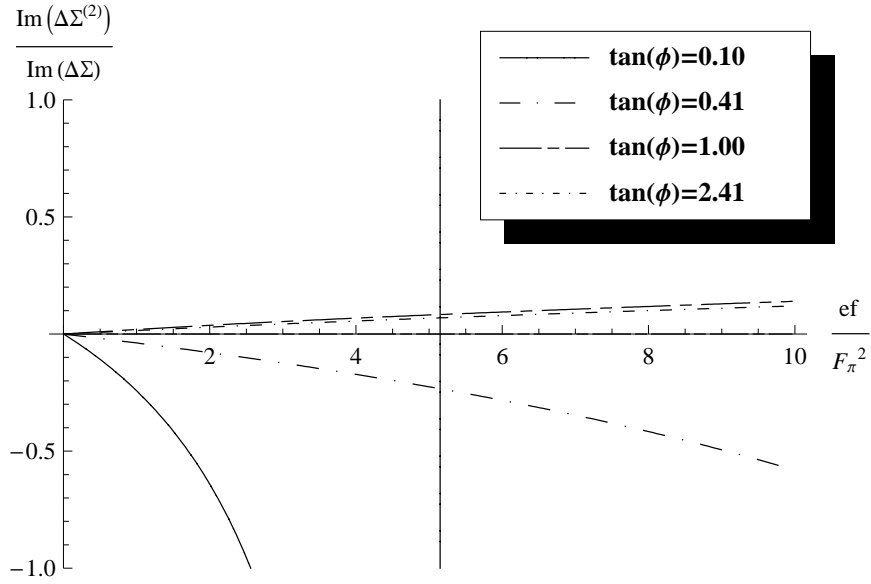
(b)

Figure 3.5: The imaginary and real parts of the ratio of the shift at two loops to the total shift for the case of general E and H fields, with f and ϕ as defined in the text. Shading depicts uncertainty due to c_{34}.

.

achieved.

The imaginary part of this integral is also revealing, as it indicates when the result is invalidated by pair creation. Here, the contribution of $\mathcal{O}(p^6)$ is more significant at larger H; while in this situation the imaginary part as a whole is smaller, the contribution to the imaginary part due to the next order result is more significant. In this regime, however, the imaginary part appears to be small enough not to invalidate the result. In a regime with a larger imaginary part, the $\mathcal{O}(p^6)$ portion is small, and therefore also not significant enough to meaningfully affect the validity of the result.

3.4   Discussion

This chapter discussed the effect of the correction at order $\mathcal{O}(p^6)$ in chiral perturbation theory to the shift in the chiral condensate in an electromagnetic field, using a finite value for M_π. The difference at $\mathcal{O}(p^4)$ between the finite M_π and the $M_\pi = 0$ result was dramatic, so an $\mathcal{O}(p^6)$ calculation was desirable in learning whether this would be the case at the next order. The $\mathcal{O}(p^6)$ result might play an important role, but the size of the correction is not qualitatively different for a finite M_π versus $M_\pi = 0$.

One interesting aspect of the $\mathcal{O}(p^6)$ extension is a tension between the large-N_C limit and the low-momentum limit as described by χPT. Terms which are lower in the chiral expansion are not necessarily lower in large-N_C QCD, and so it is possible for higher-order terms in the chiral expansion to be lower-order in N_C. Lowest-order

terms in N_C are those with no trace at all, or with no pion fields. There are no such terms which contribute to the shift in the chiral condensate due to electromagnetic fields at $\mathcal{O}(p^4)$, but at $\mathcal{O}(p^6)$, there is such a term. Higher-order terms in the chiral lagrangian can also have such low-order terms in N_C, but these are second order corrections.

Chapter 4

Directional Dependence: Magnetization at the Perturbative Scale

4.1 Introduction

The previous chapters focused on the effects of an electromagnetic field at relatively small field strength. The quantity used to probe this regime was the chiral condensate, a scalar quantity. However, electric and magnetic fields do not only shift the chiral condensate, but contain new vectorial information which did not exist before they were imposed. One of the most interesting quantities in measuring the directional effects of a magnetic field is the magnetization, which was defined in the introduction via Eq. (1.41) as

$$\mathbf{M} = \mathbf{B} - \mathbf{H} = \frac{\delta S_{eff}^{matter}}{\delta \mathbf{B}}.$$ (4.1)

This chapter will examine the magnetization of the vacuum due to a magnetic field in the perturbative regime; the calculations are based on those originally discussed in Ref. [113].

In the past, the magnetization has been studied at low-to-medium energy regimes[114], also using chiral perturbation theory, as was done in earlier chapters for the chiral condensate. These results, while not employing the full analytic result discussed here, were derived in the limits $qB \ll m_\pi^2$ and $\Lambda^2 \gg qB \gg m_\pi^2$. As discussed in Chapt. 2, the former approximation is valid, wheareas the latter will likely

remove the results from the regime of validity for χPT. In the previous chapters, this problem was solved by assuming no relationship between qB and m_π, and then applying chiral perturbation theory. Another possible solution is to take qB to be extremely large, $qB \gg \Lambda_{QCD}$, and thus place the calculation firmly within the perturbative regime. As discussed previously, realistic magnetic fields are not nearly this large, so results in this regime are not likely to be experimentally relevant, but provide another perspective on the shift in vacuum quantities.

Another important motivation for not studying the chiral condensate at high energies is that chiral symmetry becomes almost meaningless at these energies. There is a very large explicit breaking of the symmetry due to the external field, which renders the possibility of spontaneous symmetry breaking immaterial. This is in contrast to the magnetization, which has no such difficulties.

In addition to the calculation in χPT, Ref. [114] also considered the case of a strong magnetic field in the context of a model. The assumptions of this model were twofold; first, that the interactions of quarks and anti-quarks dominate the calculation of magnetization, and second, that a potential model is a good approximation for these interactions. Physically, the magnetic field causes the quarks and anti-quarks into relativistic Landau orbits in the plane perpendicular to the field, so that only one free dimension remains, and interactions between the quarks and anti-quarks must occur along this direction. When the magnetic field is strong enough, the quarks and anti-quarks form spin polarized pairs, which results in a magnetization of the vacuum. As the field gets stronger, the binding between the quark and anti-quark will become tighter, and at very strong fields, the coupling between a

tightly bound quark and anti-quark can be effectively modeled via a color coulomb potential, with the effects of perturbative QCD at this scale being taken into account via the running of the coupling. With these assumptions, then, Ref. [114] solves the interaction in the WKB approximation. In this case, the pairs are taken to be packed as closely as possible, so their density is taken to be determined by the size of the pairs. Using these approximations, the magnetization resulting from the condensation of a particular quark flavor is calculated by Ref. [114] to be

$$M \approx \frac{q^2 B \Lambda_{QCD}}{m\pi} \left(\frac{qB}{\Lambda_{QCD}^2} \right)^{\frac{1}{2} \exp(-\pi/2A))}$$

$$A = \frac{8\pi}{11N_c - 2N_f}$$

(4.2)

where m is the *constituent* quark mass and N_c and N_f are the numbers of colors and flavors respectively in the theory.

Because of these ad-hoc assumptions, however, these predictions are not as robust as might be hoped. Ref. [114] discusses these difficulties, and notes that the quantitative result could differ substantially from that derived. It also expresses the belief that the assumptions of the model are good enough to predict the qualitative behavior. One issue which affects this accuracy is the inclusion of the constituent quark mass, which is not a property of QCD, but rather a model-dependent quantity relevant at long distances. This may or may not be a problem in the regimes where the applicable model is reasonably accurate, but in the regime of strong fields, the length scales probed become smaller than the size of the constituent quark and therefore using a constituent quark mass as a parameter becomes highly suspect.

This leads to the motivation for studying the magnetization in the perturbative

regime. Because the difficulties with the approach in Ref. [114] result from its dependence upon a particular model, a model-independent approach is clearly of interest. The perturbative regime is applicable because the electromagnetic field is the only external parameter in the problem, and therefore sets the scale for the interaction. In the physical picture discussed above, then, the electromagnetic field sets the scale for the Landau orbits, and when $qB \gg \Lambda_{QCD}^2$, the orbits are small and gluon exchange is the appropriate description of the interaction. Of course, when this field is large, asymptotic freedom guarantees that these interactions will be weak. Thus, qualitatively, even though the quarks might be thought of as still being within hadrons, they are stuck in Landau orbits so small that they will only weakly interact with any other parts of the hadron. The only interactions between the quark and anti-quark relevant at such a short range is the electromagnetic interaction and the strong interaction via gluon exchange in the perturbative regime.

The directional effect of a strong external magnetic field imposed on a vacuum is measured here via the magnetization. In the first section, the magnetization at leading order is discussed, then its generalization to next-to-leading order, and the chapter concludes with a brief discussion of the results.

4.2   Magnetization at leading order

The magnetization can be calculated via Eq. (4.1). As discussed, for the case of $qB \gg \Lambda_{QCD}$, pQCD can be used to calculate the effective lagrangian. At lowest order, the effective lagrangian can be calculated using only a single quark flavor; this

is because the first order lagrangian has a only a single quark loop, which means that only a single flavor will be present in a single calculation and the calculation for each flavor is independent. Another assumption that must be addressed is that the masses of the quarks are assumed to be small, but because in this context this means that $m_q \ll qB$, this requirement is met easily. For fields large enough, the analysis will apply even to heavy quarks, as the perturbative expansion does not have an upper bound in momentum. In regions not quite so large, $eB \sim 2\text{GeV}$, the perturbative calculation will apply to the u, d, and s quarks and the contribution from the heavier quarks will be suppressed.

In pQCD, the interactions at lowest order do not involve contributions of order α_s, but rather simply use the electromagnetic interaction of the quarks with the external field. This means that the effective action is just that calculated by Schwinger, as discussed in the introduction, with the mass and charge of the particular flavor under consideration substituted for the mass and charge of the pion as discussed in prior chapters. This results in an effective lagrangian of the form [75]:

$$\mathcal{L}_{\text{eff}}^f = -\frac{N_c}{8\pi^2} \int_0^\infty \frac{ds}{s^3} e^{-m_{q_f}^2 s} \left(\frac{q_f B s}{\tanh q_f B s} - 1 - \frac{1}{3}(q_f B s)^2 \right) , \qquad (4.3)$$

where superscript $\mathcal{L}_{\text{eff}}^f$ indicates the contribution to the effective action for a particular flavor of quark, q_f is the charge for quarks of that flavor, and m_q is the *current* quark mass for that flavor.

From this expression, the magnetization is easy to obtain by taking the derivative. Changing to the dimensionless variable z for the integration yields for the

magnetization:

$$\mathbf{M}_f^{(0)} = -\frac{q_f^2 \mathbf{B} N_c}{8\pi^2} I(B, m_{q_f})$$

$$I(B, m_{q_f}) \equiv \int_0^\infty \frac{dz}{z^2} e^{-\frac{m_q^2}{qB} z} \left(\coth z - \frac{z}{\sinh^2 z} - \frac{2}{3} z \right),$$

(4.4)

where the superscript (0) indicates that the calculation is lowest order in α_s. The additional term in the integrand from the expression discussed in previous chapters, proportional to $-2/3z$, is required to renormalize the electric field and cancel divergent fermion loops. With this term, the integrand converges for $z \to 0$. In the previous chapters, it was possible to simplify similar integrals analytically. However, in this case, that is not necessary as the condition $q_f B \gg m_q^2$ can be used to greatly simplify the expression. Because its parameter is so small, the exponential in the integrand decays very slowly so that the large z region dominates the integral. The relevant part of the integral is then the part above some cutoff, c, with the properties that $c \gg 1$, $\frac{m_q^2}{q_f B} c \ll 1$; it is possible to choose a large parameter c because $\frac{m_q^2}{q_f B}$ is very small so that the hierarchy of scales is not problematic. The separated integral is then

$$I(B, m_{q_f}) = I_1 + I_2$$

$$I_1 = \int_0^c \frac{dz}{z^2} e^{-\frac{m_q^2}{q_f B} z} \left(\coth z - \frac{z}{\sinh^2 z} - \frac{2}{3} z \right)$$

(4.5)

$$I_2 = \int_c^\infty \frac{dz}{z^2} e^{-\frac{m_q^2}{q_f B} z} \left(\coth z - \frac{z}{\sinh^2 z} - \frac{2}{3} z \right).$$

As discussed, I_2, as the large-z portion of the integral, dominates. In this region, $\coth(z) \propto 1$ and $z/\sinh^2(z) \propto 4ze^{-2z}$, both of which can be dropped in comparison to the $-2/3z$ term. With only small corrections, then, the only relevant part of the

integral is

$$I(B, m_q) = -\frac{2}{3} \int_c^\infty \frac{dz}{z} e^{-m_q^2/(q_f B)z}. \tag{4.6}$$

This can be simplified straightforwardly to $I(B, m_q) = -\frac{2}{3}\Gamma^{(0)}\left(\frac{m_q^2}{q_f B}c\right)$, where $\Gamma^{(0)}(Z)$

is a plica function of zero order. This expression can be even further simplified using

the condition $\frac{m_q^2}{q_f B}c \gg 1$, yielding:

$$I(B, m_{q_f}) = -\frac{2}{3} \log\left(\frac{m_q^2}{q_f B}c\right) = \frac{2}{3} \log\left(\frac{q_f B}{\mu^2}\right) + \text{const}, \tag{4.7}$$

where μ^2 is a scale parameter. The constant in Eq. (4.7) is of the same order

as the previously neglected corrections to the integral, and can be ignored. With

this expression for the integral, the first-order magnetization correction in pQCD

becomes

$$\mathbf{M}_f^{(0)} = \frac{q_f^2 \mathbf{B} N_c}{12\pi^2} \log\frac{q_f B}{\mu^2}, \tag{4.8}$$

up to small corrections. The leading corrections to this expression are proportional

to B, rather than $B \log B$, and the choice of μ can allow these corrections to be fully

canceled. The corrections of that order contain not only perturbative corrections,

but substantial contributions from the nonperturbative region, and therefore μ also

contains nonperturbative information. However, in the case of strong fields, the

expression is only weakly dependent on μ, depending upon it only logarithmically.

4.3   Magnetization at next-to-leading order

With this leading order expression, it is instructive to consider the corrections

in more detail, through next-to-leading-order corrections. As discussed, these correc-

tions are both perturbative and nonperturbative. The nonperturbative corrections
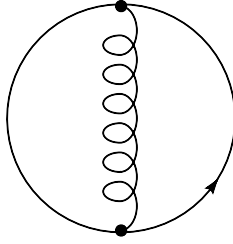
Figure 4.1: Diagram contributing to magnetization at next-to-leading order

are of course due to interactions in the low momentum region, and so should be power-law suppressed in $\Lambda_{QCD}^2/(eB)$ compared to both the leading-order result and the leading order corrections to this result. The primary corrections to Eq. (4.8) should then be perturbative. Their general form will be

$$\mathbf{M} = \mathbf{M}^{(0)} \left(1 + c_1 \alpha_s + c_2 \alpha_s^2 + \cdots \right), \tag{4.9}$$

where c_1, c_2, etc., are dimensionless constants. The strong coupling constant, α_s, is scale-dependent, and in this case should be evaluated at the only external scale in the problem, eB. This section will derive the form of the leading perturbative correction, c_1; full calculation shows that it vanishes.

As at leading order, the first step is to find the effective lagrangian, or the vacuum energy at this order. The diagram contributing at this order is depicted in Fig. 4.1. At this order, as well as in the leading order vacuum energy, the contributions from each flavor are independent, because there is still only a single quark loop contributing. Only at the next order, where there is a second quark loop and therefore a second flavor of quark, will the flavors begin to mix. The calculation is similar to any perturbative QCD calculation, with the propagator for the fermion

replaced with the the propagator for a spin-$\frac{1}{2}$ fermion in a constant magnetic field as derived by Schwinger[75]. The next-to-leading order contribution to the vacuum energy is then

$$G^{(B)}_{ij}(p) = - \delta_{ij} \int_0^\infty \frac{ds}{\cos eBs} \exp\left[-is\left(m_q^2 + p_z^2 + \frac{p_x^2 + p_y^2}{eBs\cot(eBs)} - E^2\right)\right]$$

$$\times \left([\cos(eBs) + \gamma_1\gamma_2\sin(eBs)] [\gamma_3 p_z - \gamma_0 E - m_q] + \frac{\gamma_1 p_x + \gamma_2 p_y}{\cos(eBs)} \right).$$

$$\mathcal{L}_f^{(1)}(B) = - 32\pi^2\alpha_s N_f^2 N_c \int_0^\infty ds \int_0^\infty ds' \exp\left[-(s+s')m_q^2\right] I(s, s', B, m_q)$$

$$I(s, s', B, m_q) = \frac{1}{(4\pi)^4 a_1^2 a_2^2 (b_1 - b_2)} \left\{ -\frac{a_1}{(cc')^2} + a_2 \right.$$

$$\left. + \log\left(\frac{b_1}{b_2}\right)\left(2m_q^2 a_1 a_2 + \frac{1}{b_1 - b_2}\left[\frac{a_1}{(cc')^2}b_1 - a_2 b_2\right]\right)\right\}$$

$$a_1 = s + s'$$

$$a_2 = st + s't'$$

$$b_1 = \frac{ss'}{s + s'}$$

$$b_2 = \frac{sts't'}{st + s't'}$$

$$c = \cosh(q_f Bs), c' = \cosh(q_f Bs'), t = \frac{\tanh(q_f Bs)}{q_f Bs}, t' = \frac{\tanh(q_f Bs')}{eq_f Bs'},$$

$$(4.10)$$

where the superscript (1) indicates an expression at order α_s^1.

These expressions include an expression for the quark mass, which would in general make these expressions appear suspicious, as calculations in the perturbative limit should not be dependent on the quark mass. In this case, it is a very small parameter, serving as an infrared regulator of the integrals.

Without some modification, $I(s, s', B, m_q)$ appears to be divergent. Fortu-

nately, the only relevant part of this integral is its dependence on the B field. It is straightforward to subtract the value of the integral for $B \to 0$, which will not affect the magnetization as it is dependent on the derivative with respect to B (and must furthermore be zero for $B = 0$). The non-divergent part of the effective lagrangian depending upon B is then

$$\mathcal{L}_{\text{eff}}^{(1)}(B) = -32\pi\alpha_s N_f^2 N_c \int_0^\infty ds \int_0^\infty ds' \exp\left[-(s+s')m_q^2\right] \left(I(s, s', B, m_q) - I(s, s', 0, m_q)\right).$$

(4.11)

While the integral is convergent, there is no straightforward way to evaluate it analytically. Again, however, as with the leading order correction, this expression can be greatly simplified in the regime of interest, $eB \gg m_q^2$. This is done using the same method as previously by dividing the integral into high-s and low-s regimes at the (dimensionful) scale $s = 1/m_0^2$. Taking the high-s part of both integrals then yields the expression

$$\mathcal{L}_f^{(1)}(B) = -32\pi\alpha_s N_f^2 N_c (q_f B) \frac{m_0^2}{2(4\pi)^4} \text{Ei}\left(-2\frac{m_q^2}{m_0^2}\right)\left(2 - 2e^{-\frac{m_q^2}{m_0^2}} + \left(\frac{m_q^2}{m_0^2}\right)\Gamma\left(0, \frac{m_q^2}{m_0^2}\right)\right),$$

(4.12)

again up to small corrections. The regime $m_0 \gg m_q$ (equivalent to the limit $q_f Bc \ll 1$ above) will yield further simplifications. Making these, then taking the derivative with respect to B, yields the next-order correction for the magnetization in the form

$$\mathbf{M}_f^{(1)}(B) = \pi\alpha_s N_c (q_f^2 \mathbf{B}) \frac{m_q^2}{q_f B} \frac{1}{16\pi^4}\left(\log\frac{eB}{\mu^2}\right)^2,$$

(4.13)

where again, μ is a renormalization scale chosen to minimize the nonperturbative corrections.

The magnetization at both leading and next-to-leading order can be combined in the form

$$\mathbf{M}_f(B) = q_f^2 \mathbf{B} \frac{N_c}{12\pi^2} \log \frac{q_f B}{\mu^2} \left(1 + 4\pi\alpha_s \frac{m_q^2}{q_f B} \frac{3}{16\pi^2} \log\left(\frac{q_f B}{\mu^2}\right)\right), \qquad (4.14)$$

plus corrections of order α_s^2.

The dependence of the result on m_q is here made manifest. A meaningful result should not be dependent upon that value, and so the fact that the result multiplies $\alpha_s m_q^2/(q_f B)$ rather than α_s is troubling, as indicates that the result is power-law suppressed in B, or that the coefficient c_1 is zero. For light quarks, the correction is not reliable at all, because its magnitude is so small, and will be dominated by the (unknown) nonperturbative correction. For heavy quarks, on the other hand, the correction is more likely to be reliable (though the fields must be stronger to satisfy the relationship $q_f B \gg m_q^2 \gg \Lambda_{QCD}^2$), and will be the leading order correction for these. In either case, the leading order result of Eq. (4.8) is accurate up to corrections of order α_s^2.

4.4   Discussion

This chapter examines the magnetization of the vacuum in the region where perturbative QCD is valid, $eB \gg \Lambda_{QCD}$, in contrast to previous chapters, which focused on the effects of weaker electromagnetic field. The contribution from each flavor can be determined independently. When eB is either much greater or much smaller than all of the quark masses, their contributions are identical, and the total contribution to the magnetization can be written as a sum of the individual

contributions as

$$\mathbf{M}(B) = \left(\sum_{\substack{\text{active} \\ \text{flavors}}} \frac{q_f^2}{e^2} \right) \mathbf{e^2 B} \frac{1}{4\pi^2} \log \frac{eB}{\mu^2} \left(1 + \mathcal{O}(\alpha_s^2) \right), \qquad (4.15)$$

where the active flavors are those whose squared mass is well below eB.

The lack of perturbative correction in this result is puzzling. There may be some deep reason for the lack of next-to-leading order correction, but at present it is unclear what this might be.

Regardless, the leading order result is a model independent calculation of the magnetization, and as such can be compared to the prior result obtained by Ref. [114] using a quark potential model and repeated in Eq. (4.2). The qualitative behavior of the two is naively very similar, as the form for both is a function linear in B times a function which increases very slowly as a function of B/Λ (in the case of the prior result, the constituent quark mass m is $\mathcal{O}(\Lambda)$). This slowly increasing function is logarithmic in the case of the perturbative expansion, and in the case of the model, is a power law with an extremely small exponent. This apparent similarity does not extend as far as it might seem, however.

For comparison, the large-N_c expansion used in the previous chapters can again be invoked. As before, it is an interesting tool useful in analyzing the qualitative behavior of various phenomena; the N_c order of various expressions can be helpful in determining how similar they are in origin. Expressions with dissimilar orders of N_c, while appearing to be very close otherwise, are likely based on very different physics. In this case, the expression derived in perturbative QCD, Eq. (4.14), is proportional to N_c. Because the expansion is based on quark degrees of freedom, it is not difficult

to understand the root of this dependence. The quarks are approximately free, so the single quark loop in the expansion contributes this single factor of N_c. The expression based on the quark model in Eq. (4.2), however, has no N_c dependence at all. In that case, while the model was based in part on the potential between a quark and an anti-quark, the expression for the actual magnetization is based on the condensed quark-anti-quark pairs, which are color singlet, and therefore do not contribute a factor of N_c. And, of course, although the power law in Eq. (4.2) is small, when the fields become extremely large, the power law will eventually become substantially larger than the logarithmic expression of Eq. (4.14).

Ultimately, the perturbative result should be more reliable than the model-based calculation as energies increase. The physical picture which justifies the perturbative expansion only becomes more valid as the strength of the field increases; the Landau orbits of the quarks become even smaller, such that they can even more accurately be approximated as being free for the purposes of vacuum polarization. In contrast, the model result of Eq. (4.2) is less justifiable in the regime of large fields. Because the quarks can be approximated as being free due to their small Landau orbits, it is less likely for them to condense with anti-quarks and form color singlet pairs for vacuum polarization. In fact, the presence of the constituent mass in the expression was a clue to this breakdown; the constituent mass is only a meaningful expression at lower energies, and at higher energies becomes an inappropriate description of quark dynamics.

The magnetization is thus one of many vacuum quantities which can be of interest in studying QCD. Like in all quantum field theories, the vacuum of QCD is

nontrivial, but the ideal quantity for measuring this structure changes at different energies. At low energies, the chiral condensate can be used, and as the order parameter for chiral symmetry breaking, it is desirable to measure it wherever it can be used. For an electromagnetic field at perturbative scales, however, the strength of the field which has pushed the calculation into the perturbative regime is high enough that there is a large explicit breaking of chiral symmetry, and another parameter must be used. The parameter here, magnetization, is of interest because, of course, it is intimately related to electromagnetism. It differs from the chiral condensate in that it is a vectorial quantity, which is interesting because it captures the vectorial nature of the applied field.

Previous chapters discussed the effects of the electromagnetic field on the vacuum of QCD at lower energies and used the chiral condensate to measure these effects. In Chapt. 2, the effects of an electromagnetic field at intermediate strengths was discussed using primarily chiral perturbation theory, though other models were also discussed. In general, all methods show the electric field to suppress the chiral condensate, whereas the magnetic field enhances it. In Chapt. 3, the effects of the electromagnetic field were examined to next-order in chiral perturbation theory, with the idea that this will extend the region of validity to slightly higher energies. It is possible that the next order correction could be significant, but because of the high error on the $\mathcal{L}_6$ coefficients in χPT, it is not possible to determine how significant at this time. In both of these first chapters, a large enough electric field invalidates the result for the shift in the chiral condensate due to pair creation, or instability of the vacuum. Finally, the current chapter discusses the magnetization of the QCD

108

vacuum at field strengths large enough to push the calculation into the perturbative regime due to magnetic fields, which has the expected form for the first order result in perturbation theory, but the next-order result in perturbation theory is small enough that non-perturbative corrections become impossible to ignore.

Bibliography

[1] K. Rajagopal and F. Wilczek, (2000), hep-ph/0011333.

[2] M. Peskin and D. Schroeder, *An Introduction to Quantum Field Theory* (Westview Press, 1995).

[3] S. Narison, *QCD as a Theory of Hadrons* (Cambridge University Press, 2004).

[4] M. Gell-Mann, Phys.Lett. **8**, 214 (1964).

[5] G. Zweig, CERN-TH-401 (1964).

[6] M. Gell-Mann, Acta Phs.Austriaca Suppl. **9**, 733 (1972).

[7] H. Fritzsch and M. Gell-Mann, Current algebra: Quarks and what else?, in *Proceedings of the XVI International Conference on High Energy Physics*, edited by J. Jackson and A. Roberts, pp. 135–165, Natl Accelerator Laboratory, 1972.

[8] H. Fritzsch, M. Gell-Mann, and H. Leutwyler, Phys.Lett. **B47**, 365 (1973).

[9] M. Han and Y. Nambu, Phys.Rev. **139**, B1006 (1965).

[10] O. W. Greenberg, Phys. Rev. Lett. **13**, 598 (1964).

[11] M. Y. Han and Y. Nambu, Phys. Rev. **139**, B1006 (1965).

[12] H. Politzer, Phys.Rev.Lett. **30**, 1346 (1973).

[13] D. Gross and F. Wilczek, Phys.Rev. **D8**, 3633 (1973).

[14] C.-N. Yang and R. L. Mills, Phys. Rev. **96**, 191 (1954).

[15] H. Weyl, Z.Phys. **56**, 330 (1929).

[16] C. Yang and R. Mills, Phys.Rev. **96**, 191 (1954).

[17] S. Weinberg, Physica **A96**, 327 (1979).

[18] J. Gasser and H. Leutwyler, Annals Phys. **158**, 142 (1984).

[19] J. Gasser and H. Leutwyler, Nucl.Phys. **B250**, 465 (1985).

[20] S. Klevansky, Rev.Mod.Phys. **64**, 649 (1992).

[21] M. Gell-Mann and M. Levy, Nuovo Cim. **16**, 705 (1960).

[22] G. 't Hooft, Nucl.Phys. **B72**, 461 (1974).

[23] G. 't Hooft, Nucl.Phys. **B75**, 461 (1974).

[24] E. Witten, Nucl.Phys. **B160**, 57 (1979).

[25] J. Erlich, E. Katz, D. Son, and M. Stephanov, Phys.Rev.Lett. **95**, 261602 (2005).

[26] C. Callan, Phys.Rev. **D2**, 1541 (1970).

[27] K. Symanzik, Commun.Math.Phys. **18**, 227 (1970).

[28] J. Bjorken, Phys.Rev. **179**, 1547 (1969).

[29] G. Altarelli and G. Parisi, Nucl. Phys. **B126**, 298 (1977).

[30] C. A. et al., Phys.Lett. **B667**, 1 (2008).

[31] K. G. Wilson, Phys. Rev. **D10**, 2445 (1974).

[32] G. Ecker, Prog.Part.Nucl.Phys. **35**, 1 (1995).

[33] A. Pich, Rept.Prog.Phys. **58**, 563 (1995).

[34] H. Dosch and S. Narison, Phys.Lett. **B417**, 173 (1998).

[35] J. Goldstone, Nuovo Cim. **19**, 154 (1961).

[36] H. Georgi, Ann.Rev.Nucl.Part.Sci. **43**, 209 (1993).

[37] J. Bijnens, G. Colangelo, and G. Ecker, JHEP **9902**, 020 (1999).

[38] J. Bijnens, G. Colangelo, and G. Ecker, Annals Phys. **280**, 100 (2000).

[39] J. Bijnens, Prog. Part. Nucl. Phys. **58**, 521 (2007), hep-ph/0604043.

[40] S. R. Sharpe and J. Singleton, Robert L., Phys. Rev. **D58**, 074501 (1998), hep-lat/9804028.

[41] W.-J. Lee and S. R. Sharpe, Phys. Rev. **D60**, 114503 (1999), hep-lat/9905023.

[42] S. Hashimoto, Int. J. Mod. Phys. **A20**, 5133 (2005), hep-ph/0411126.

[43] R. Hagedorn, Nuovo Cim.Suppl. **3**, 147 (1965).

[44] R. Hagedorn and J. Ranft, Nuovo Cim.Suppl. **6**, 169 (1968).

[45] K. Huang and S. Weinberg, Phys.Rev.Lett. **25**, 895 (1970).

[46] J.-R. Cudell and K. Dienes, Phys.Rev.Lett. **69**, 1324 (1992).

[47] K. Dienes and J.-R. Cudell, Phys.Rev.Lett. **69**, 1324 (1992).

[48] W. Broniowski and W. Florkowski, Phys.Rev. **D70**, 117503 (2004).

[49] Y. Nambu and G. Jona-Lasinio, Phys.Rev. **122**, 345 (1961).

[50] Y. Nambu and G. Jona-Lasinio, Phys.Rev. **124**, 246 (1961).

[51] M. Goldberger and S. Treiman, Phys.Rev. **110**, 1178 (1958).

[52] M. Gell-Mann, R. Oakes, and B. Renner, Phys.Rev. **175**, 2195 (1968).

[53] J. Collins and M. Perry, Phys.Rev.Lett. **34**, 1353 (1975).

[54] D. H. Rischke, Prog. Part. Nucl. Phys. **52**, 197 (2004), nucl-th/0305030.

[55] F. Karsch and M. Lutgemeier, Nucl.Phys. **B50**, 449 (1999).

[56] M. C. et al., Phys.Rev. **D74**, 054507 (2006).

[57] M. Asakawa and K. Yazaki, Nucl.Phys. **A504**, 1989 (1989).

[58] A. Barducci, R. Casalbuoni, S. D. Curtis, R. Gatto, and G. Pettini, Phys.Lett. **B231**, 463 (1989).

[59] A. Barducci, R. Casalbuoni, G. Pettini, and R. Gatto, Phys.Rev. **D49**, 426 (1994).

[60] M. Stephanov, K. Rajagopal, and E. Shuryak, Phys.Rev.Lett. **81**, 4816 (1998).

[61] A. Halasz, A. Jackson, R. Shrock, M. Stephanov, and J. Verbaarschot, Phys.Rev. **D58**, 096007 (1998).

[62] J. Berges and K. Rajagopal, Nucl.Phys. **B538**, 215 (1999).

[63] P. Hasenfratz and F. Karsch, Phys. Lett. **B125**, 308 (1983).

[64] U. W. Heinz and P. F. Kolb, Nucl. Phys. **A702**, 269 (2002), hep-ph/0111075.

[65] D. Teaney, J. Lauret, and E. V. Shuryak, (2001), nucl-th/0110037.

[66] J. O. Andersen, E. Braaten, and M. Strickland, Phys. Rev. Lett. **83**, 2139 (1999), hep-ph/9902327.

[67] M. Buballa, Phys. Rept. **407**, 205 (2005), hep-ph/0402234.

[68] E. Braaten and A. Nieto, Phys. Rev. **D51**, 6990 (1995), hep-ph/9501375.

[69] J. Bardeen, L. Cooper, and J. Schrieffer, Phys.Rev. **106**, 162 (1957).

[70] J. Bardeen, L. Cooper, and J. Schrieffer, Phys.Rev. **108**, 1175 (1957).

[71] B. Barrois, Nucl.Phys. **B129**, 390 (1977).

[72] D. Bailin and A. Love, Phys.Rept. **107**, 325 (1984).

[73] M. Alford, K. Rajagopal, and F. Wilczek, Phys.Lett. **B422**, 247 (1998).

[74] R. Rapp, T. Schafer, E. Shuryak, and M. Velkovsky, Phys.Rev.Lett. **81**, 53 (1998).

[75] J. S. Schwinger, Phys. Rev. **82**, 664 (1951).

[76] S. P. Klevansky and R. H. Lemmer, Phys. Rev. **D39**, 3478 (1989).

[77] G. Baym and C. Pethick, Ann.Rev.Astron.Astrophys. **17**, 415 (1979).

[78] STAR, I. V. Selyuzhenkov, Rom. Rep. Phys. **58**, 049 (2006), nucl-ex/0510069.

[79] D. Kharzeev, Phys. Lett. **B633**, 260 (2006), hep-ph/0406125.

[80] D. E. Kharzeev, L. D. McLerran, and H. J. Warringa, Nucl. Phys. **A803**, 227 (2008), 0711.0950.

[81] J. Lattimer and M. Prakesh, Science **304**, 536 (2004).

[82] A. Nikishov, Nucl.Phys. **B21**, 346 (1970).

[83] D. Allor, T. Cohen, and D. McGady, (2008).

[84] T. Cohen and D. McGady, Phys.Rev. **D78**, 036008 (2008).

[85] F. Cooper and E. Mottola, Mod. Phys. Lett. **A2**, 635 (1987).

[86] F. Cooper and E. Mottola, Phys. Rev. **D40**, 456 (1989).

[87] Y. Kluger, J. M. Eisenberg, B. Svetitsky, F. Cooper, and E. Mottola, Phys. Rev. Lett. **67**, 2427 (1991).

[88] Y. Kluger, J. M. Eisenberg, B. Svetitsky, F. Cooper, and E. Mottola, Phys. Rev. **D45**, 4659 (1992).

[89] J. C. R. Bloch *et al.*, Phys. Rev. **D60**, 116011 (1999), nucl-th/9907027.

[90] R.-C. Wang and C. Y. Wong, Phys. Rev. **D38**, 348 (1988).

[91] W. Pauli and F. Villars, Rev. Mod. Phys. **21**, 434 (1949).

[92] A. Y. Babansky, E. V. Gorbar, and G. V. Shchepanyuk, Phys. Lett. **B419**, 272 (1998), hep-th/9705218.

[93] A. Goyal and M. Dahiya, Phys. Rev. **D62**, 025022 (2000), hep-ph/9906367.

[94] S. Schramm, B. Muller, and A. J. Schramm, Mod. Phys. Lett. **A7**, 973 (1992).

[95] K. G. Klimenko, Z. Phys. **C54**, 323 (1992).

[96] K. G. Klimenko, (1998), hep-ph/9809218.

[97] D. Ebert, K. G. Klimenko, M. A. Vdovichenko, and A. S. Vshivtsev, Phys. Rev. **D61**, 025005 (2000), hep-ph/9905253.

[98] V. P. Gusynin, V. A. Miransky, and I. A. Shovkovy, Phys. Rev. Lett. **73**, 3499 (1994), hep-ph/9405262.

[99] V. P. Gusynin, V. A. Miransky, and I. A. Shovkovy, Phys. Lett. **B349**, 477 (1995), hep-ph/9412257.

[100] T. D. Cohen, D. A. McGady, and E. S. Werbos, Phys. Rev. **C76**, 055201 (2007), 0706.3208.

[101] I. A. Shushpanov and A. V. Smilga, Phys. Lett. **B402**, 351 (1997), hep-ph/9703201.

[102] T. D. Cohen and R. F. Lebed, Phys. Rev. **D74**, 056006 (2006), hep-ph/0608038.

[103] T. D. Cohen and W. Broniowski, Phys. Lett. **B292**, 5 (1992), hep-ph/9208253.

[104] T. D. Cohen, Phys. Lett. **B359**, 23 (1995), hep-ph/9505427.

[105] T. D. Cohen, Phys. Lett. **B554**, 28 (2003), hep-ph/0210278.

[106] T. D. Cohen, Rev. Mod. Phys. **68**, 599 (1996).

[107] A. Jeffrey and D. Zwillinger, editors, *Table of Integrals, Series, and Products* (Academic Press, 2007).

[108] T. D. Cohen and D. A. McGady, Phys. Rev. **D78**, 036008 (2008), 0807.1117.

[109] N. O. Agasian and I. A. Shushpanov, Phys. Lett. **B472**, 143 (2000), hep-ph/9911254.

[110] E. S. Werbos, Phys. Rev. **C77**, 065202 (2008), 0711.2635.

[111] S. Bellucci, J. Gasser, and M. E. Sainio, Nucl. Phys. **B423**, 80 (1994), hep-ph/9401206.

[112] J. Bijnens and P. Talavera, Nucl. Phys. **B489**, 387 (1997), hep-ph/9610269.

[113] T. D. Cohen and E. S. Werbos, (2008), 0810.5103.

[114] D. N. Kabat, K.-M. Lee, and E. J. Weinberg, Phys. Rev. **D66**, 014004 (2002), hep-ph/0204120.